For submission to *Organometallics*

Photoactivatable Organometallic Pyridyl Ruthenium(II) Arene Complexes

Soledad Betanzos-Lara,[a†] Luca Salassa,[a] Abraha Habtemariam,[a] Olga Nováková,[b] Ana M. Pizarro,[a] Guy J. Clarkson,[a] Barbora Liskova,[b] Viktor Brabec,[b] and Peter J. Sadler [a]*

[a]*Department of Chemistry, University of Warwick, Coventry, UK CV4 7AL;* [b]*Institute of Biophysics, Academy of Sciences of the Czech Republic, v.v.i., Kralovopolska 135, CZ61265 Brno, Czech Republic*

E-mail: P.J.Sadler@warwick.ac.uk

[†]*Current address: Departamento de Química Inorgánica, Facultad de Química, Universidad Nacional Autónoma de México (UNAM), Ciudad Universitaria, Coyoacán, México, D.F. 04510 México*

The synthesis and characterization of a family of piano-stool Ru^{II} arene complexes of the type [(η^6-arene)Ru(N,N')(L)][PF_6]$_2$ where arene is *para*-cymene (*p*-cym), hexamethylbenzene (hmb) or indane (ind); N,N' is 2,2'-bipyrimidine (bpm), 1,10-phenanthroline (phen), 1,10-phenanthroline-5,6-dione (phendio), 4,7-diphenyl-1,10-phenanthroline (bathophen), and L is pyridine (Py), 4-methylpyridine (4-MePy), 4-methoxypyridine (4-MeOPy), 4,4'-bipyridine (4,4'-biPy), 4-phenylpyridine (4-PhPy), 4-benzylpyridine (4-BzPy), 1,2,4-triazole (trz), 3-acetylpyridine (3-AcPy), nicotinamide (NA), or 3-acetatepyridine (3-AcOPy) are reported; including the X-ray crystal structures of [(η^6-*p*-

cym)Ru(bpm)(4-MePy)]$^{2+}$ (**2**), [(η^6-*p*-cym)Ru(bpm)(4-BzPy)]$^{2+}$ (**6**), [(η^6-*p*-cym)Ru(bpm)(trz)]$^{2+}$ (**7**), [(η^6-*p*-cym)Ru(phen)(Py)]$^{2+}$ (**10**), and [(η^6-ind)Ru(bpy)(Py)]$^{2+}$ (**13**). These complexes can selectively photodissociate the monodentate ligand (L) when excited with UVA or white light allowing strict control of the formation of the reactive aqua species [(η^6-arene)Ru(N,N')(OH_2)]$^{2+}$ that otherwise would not form in the dark. The photoproducts were characterized by UV-vis absorption and ^{1}H NMR spectroscopy. DFT and TD-DFT calculations were employed to characterize the excited states and to obtain information on the photochemistry of the complexes. All the Ru^{II} pyridine complexes follow a relatively similar photochemical L-ligand dissociation mechanism, likely to occur from a series of ^{3}MC triplet states with dissociative character. The photochemical process proved to be much more efficient when UVA-range irradiation was used. More strikingly, light activation was used to photo-trigger binding of these potential anticancer agents with discriminating preference towards 9-ethylguanine (9-EtG) over 9-ethyladenine (9-EtA). Calf-thymus (CT)-DNA binding studies showed that the irradiated complexes bind to CT-DNA whereas the non-irradiated forms, bind negligibly. Studies of CT-DNA interactions in cell-free media suggest combined weak monofunctional coordinative and intercalative binding modes. The Ru^{II} arene complexes [(η^6-*p*-cym)Ru(bpm)(Py)]$^{2+}$ (**1**), [(η^6-*p*-cym)Ru(bpm)(4-MeOPy)]$^{2+}$ (**3**), [(η^6-*p*-cym)Ru(4,4'-biPy)]$^{2+}$ (**4**), [(η^6-hmb)Ru(bpm)(Py)]$^{2+}$ (**8**), [(η^6-ind)Ru(bpm)(Py)]$^{2+}$ (**9**), [(η^6-*p*-cym)Ru(phen)(Py)]$^{2+}$ (**10**), [(η^6-*p*-cym)Ru(bathphen)(Py)]$^{2+}$ (**12**), [(η^6-*p*-cym)Ru(bpm)(NA)]$^{2+}$ (**15**), and [(η^6-*p*-cym)Ru(bpm)(3-AcOPy)]$^{2+}$ (**16**) were cytotoxic towards A2780 human ovarian cancer cell lines in the absence of photoirradiation (IC_{50} values in the range of 9.0–60 μM).

Introduction

Photochemical activation is an attractive approach for achieving precise spatial and temporal control of the biological action of transition metal complexes that behave as inactive drugs in the dark.[1] Such a strategy has been applied to (poly)pyridyl complexes as diagnostic and therapeutic agents.[2,3,4] The basic

rationale involves the modification of the Ru^{II} molecules by introducing a group that can be selectively cleaved by the absorption of light, promoting its release and offering the possibility of controlling the location, timing, and dosage of the therapeutic metal complex. This requires breaking of a coordination bond by the use of high energy UV-visible light photons. The photochemistry of half-sandwich species such as $[(\eta^6\text{-}C_6H_6)Ru(\eta^5\text{-}C_5H_5)]^+$ has been investigated.[5] Photosubstitution of the arene is the dominant reaction pathway and benzene is released. Irradiation in aqueous solution of Ru^{II} complexes of the form $[(\eta^6\text{-arene})Ru(L)_3]^{2+}$ where arene = benzene, toluene, or isopropyltoluene; and L = NH_3 or H_2O, was found to lead in each case to the substitution of the arene by water molecules as the only observable photoreaction to produce $[Ru(OH_2)_3L_3]^{2+}$ plus the corresponding free arene.[6] Other investigations have reported that $[(\eta^6\text{-arene})Ru(P(n\text{-}Bu)_3)Cl_2]$ dissolved in aromatic solvents undergoes exchange of coordinated and solvent arenes when irradiated with UVA.[7] A few dinuclear complexes based on the typical half-sandwich motif have been also studied. Amongst them, the complex $[\{(\eta^6\text{-ind})Ru(Cl)\}_2(\mu\text{-}2,3\text{-dpp})_2]^{2+}$ where dpp is 2,3-bis(2-pyridyl)pyrazine[8] releases the arene upon irradiation generating vacant coordination sites that make it more reactive towards DNA binding.

Related complexes of general formula $[(\eta^6\text{-arene})Ru(XY)Z]^{n+}$ where XY is a bidentate chelating ligand and Z is a leaving group (typically an halogen), have been extensively investigated for their promising cytotoxic properties towards various cancer cell lines.[9,10] A crucial step in one mode of activation of these anticancer agents is generally the initial aquation of the Ru–Z bond to form a more reactive aqua specie,[11] which subsequently can bind to biological targets. It has been shown previously that fast hydrolysis rates can usually lead to non-cytotoxic complexes, whereas very slow hydrolysis rates often lead to low *in vitro* cytotoxicity,[10,12] for example the complex $[(\eta^6\text{-hmb})Ru(en)Py]^{2+}$ does not hydrolyze in aqueous solution at 310 K and is not cytotoxic (IC_{50} value > 100 μM).[11]

We have recently shown that one key strategy to increase the potential of this class of complexes is to activate the release of the monodentate ligand Z by photoirradiation to promote the formation of the aqua adduct, which would otherwise not form in the dark.[13] The work reported here is concerned with

the synthesis and characterization of an extended series of organometallic Ru^{II} complexes of the form $[(\eta^6\text{-arene})Ru(N,N')(L)][PF_6]_2$ where N,N' is a bidentate chelating ligand and L is a pyridine or pyridine-derivative ligand that can be selectively dissociated upon photoirradiation, Figure 1. Their behavior in the dark and under photoirradiation in aqueous solution, as well as in the presence of nucleobases such as 9-ethylguanine (9-EtG) and 9-ethyladenine (9-EtA) has been investigated. A description of the excited states for all the Ru^{II} arene complexes was obtained with the aid of Density Functional Theory (DFT) and Time-Dependent DFT (TD-DFT) calculations.[14] Finally, their potential as cytotoxic agents was also investigated as a preliminary approach towards full photocytotoxicity investigations by performing cell growth inhibition assays (IC_{50} values) in various human cancer cell lines in the absence of irradiation and also by studying their interactions with DNA in cell-free media, both in the dark and upon photoirradiation.

Experimental Section

Materials. $RuCl_3 \cdot 3H_2O$ was purchased from Precious Metals Online (PMO Pty Ltd) and used as received. 2,2'-bipyrimidine (bpm), 1,10-phenanthroline (phen), 1,10-phenanthroline-5,6-dione (phendio), 4,7-diphenyl-1,10-phenanthroline (bathophen), pyridine (Py), 4-methylpyridine (4-Mepy), 4-methoxypyridine (4-MeOPy), 4,4'-bipyridine (4,4'-biPpy), 4-phenylpyridine (4-PhPy), 4-benzylpyridine (4-BzPy), 1,2,4-triazole (trz), 3-acetylpyridine (3-AcPy), nicotinamide (NA), 3-acetatepyridine (3-AcOPy), 9-ethylguanine (9-EtG), 9-ethyladenine (9-EtA) and KPF_6 were obtained from Sigma-Aldrich. The Ru^{II} halido mononuclear precursors $[(\eta^6\text{-arene})Ru(N,N')Cl][PF_6]$, where arene is *para*-cymene (*p*-cym), hexamethylbenzene (hmb) or indane (ind); N,N' is bpm, phen, phendio, bathophen, or bpy were synthesized according to a previously reported method.[15] The solvents used for photochemistry and UV-vis absorption spectroscopy were dry methanol (reagent grade) and deionized water. For NMR spectroscopy the solvents used were acetone-d_6, DMSO-d_6, methanol-d_4 and D_2O obtained from Aldrich. All chemicals were used without further purification.

Synthesis of Ruthenium Complexes. Complexes of the form $[(\eta^6\text{-arene})Ru(N,N')(L)][PF_6]_2$ where arene is *p*-cym, hmb, or ind; N,N' is bpm, phen, phendio, bathophen, or bpy; and L is Py, 4-MePy, 4-MeOPy, 4,4'-biPy, 4-PhPy, 4-BzPy, trz, 3-AcPy, NA, or 3-AcOPy were synthesized using a previously described procedure;[9] the details and characterization are given in the Supporting Information. Complex **1** (L = Py) has been previously reported by us.[13] Suitable crystals for X-ray crystallography were obtained from a saturated acetone solution at 278 K for complexes $[(\eta^6\text{-}p\text{-cym})Ru(bpm)(4\text{-MePy})]^{2+}$ (**2**), and $[(\eta^6\text{-}p\text{-cym})Ru(bpm)(4\text{-BzPy})]^{2+}$ (**6**), from a saturated acetone-d_6 solution at 298 K for complex $[(\eta^6\text{-}p\text{-cym})Ru(bpm)(trz)]^{2+}$ (**7**), and of $[(\eta^6\text{-ind})Ru(bpy)(Py)]^{2+}$ (**13**) by slow diffusion of Et_2O at 298 K.

X-ray Crystallography. Diffraction data were collected either on an Oxford Diffraction Gemini four-circle system with a Ruby CCD area detector or on a Siemens SMART three-circle system with CCD area detector equipped with an Oxford Cryosystem Cryostream Cooler. All structures were refined by full-matrix least squares against F^2 using SHELXL 97.[16] The structures of complexes **2**, **6**, **7**, **10** and **13** were solved by direct methods using SHELXS[17] (TREF) with additional light atoms found by Fourier methods. Hydrogen atoms were added at calculated positions and refined using a riding model with freely rotating methyl groups. Anisotropic displacement parameters were used for all non-H atoms; H-atoms were given isotropic displacement parameters equal to 1.2 (or 1.5 for methyl hydrogen atoms) times the equivalent isotropic displacement parameter of the atom to which the H-atom is attached.

X-ray crystallographic data for complexes **2**·$[PF_6]_2$, **6**·$[PF_6]_2$, **7**·$[PF_6]_2$, **10**·$[PF_6]_2$ and **13**·$[PF_6]_2$ are available as Supporting Information and have been deposited in the Cambridge Crystallographic Data Centre under the accession numbers CCDC 855333, 855330, 855331, 855334, 855332, respectively. X-ray crystallographic data in CIF format are available from the Cambridge Crystallographic Data Centre (http://www.ccdc.cam.ac.uk/).

NMR Spectroscopy. ^1H and ^{13}C NMR spectra were acquired in 5 mm NMR tubes at 298 K (unless otherwise stated) on either a Bruker DRX-500, Bruker AV III 600 or Bruker AV II 700 NMR spectrometers. All data processing was carried out using XWIN-NMR version 3.6 (Bruker U.K. Ltd.).

^{1}H NMR chemical shifts were internally referenced to TMS *via* 1,4-dioxane (δ = 3.71) or residual $CHCl_3$ (δ = 7.27), MeOH (δ = 3.31) or DMSO (δ = 2.50). 1D spectra were recorded using standard pulse sequences. Typically, data were acquired with 128 transients into 16k data points over a spectral width of 14 ppm. 2D COSY or TOCSY and NOESY spectra were recorded using standard pulse-pulse sequences. Typically, the data were acquired with 72 transients into 2048 k data points over a spectral width of 14 ppm using a relaxation delay of 1.5 s and a mixing time of 0.4–0.6 s. ^{1}H NMR signals were referenced to dioxane as an internal reference (δ = 3.71).

Elemental Analysis. Elemental analyses were performed by the Warwick Analytical Service which is the analytical division of Exeter Analytical (U.K. Ltd.) using an Exeter Analytical Elemental Analyzer (CE440).

High Resolution Electrospray Mass Spectrometry (HR-MS). HR-MS data were obtained on a Bruker MaXis UHR-TOF. All the samples were analyzed by positive-ion ESI(+) mass spectrometry. Samples were prepared either in 100% H_2O or 95% MeOH/5% H_2O mixture and typically injected at 2 μL min^{-1}, nebulizer gas (N_2) 0.4 bar, dry gas (N_2) 4 L min^{-1} and dry temp 180 ºC, Funnel RF 200V, Multiple RF 200, quadrupole ion energy 4 eV, collision cell 5 eV, ion cooler RF settings, ramp from 50 to 250 V.

UV-vis Absorption Spectroscopy. UV-vis absorption spectra were recorded on a Cary 300-spectrophotometer using 1-cm pathlength quartz cuvettes (600 μL) and a PTP1 Peltier temperature controller. Spectra were recorded at 310 K in deionized water from 200 to 800 nm and were processed using Cary WinUV software for Windows XP. Absorption spectra of CT-DNA/ruthenium(II) complexes solutions were obtained with a Beckman DU 7 4000 UV-Vis spectrophotometer equipped with a thermoelectrically controlled cell holder and 1-cm pathlength quartz cells.

pH* Measurements. pH values were measured at ambient temperature using a Corning 240 pH meter equipped with a micro combination KNO_3 (chloride free) electrode calibrated with Aldrich buffer solutions of pH 4, 7, and 10. The pH* values (pH meter reading without correction for effects of

deuterium on glass electrode)[18] of NMR samples in D_2O were measured at about 298 K directly in the NMR tube, before and after recording NMR spectra, using the same method. The pH* values were adjusted with dilute NaOH or HNO_3 solutions in D_2O.

Photoirradiation of Ru^{II} Arene Complexes. Aqueous solutions of the Ru^{II} arene complexes were photoirradiated at 310 K using the photoreactor LZC 4V Illuminator (Luzchem, Canada) with temperature controller and UVA (λ_{irr} = 320−400 nm with a maximum intensity at ~360 nm, 1 J cm^{-2} h^{-1}) or white light lamps (λ_{irr} = 400−660 nm providing average light power of 1 J cm^{-2} h^{-1}). UV-vis absorption spectra of 100 μM solutions in deionized water or ^1H NMR spectra of 300 mM solutions in D_2O of the Ru^{II} arene complexes were recorded as previously stated (*vide supra*) at different stages of photoirradiation. Solutions were stored in the dark to minimize unwanted photoreactions between measurements.

Computational Details. Gaussian 03 (G03) program[19] employing the DFT method, Becke three parameter hybrid functional, and Lee-Yang-Parr's gradient corrected correlation functional (B3LYP)[20] were used. The LanL2DZ basis set[21] and effective core potential were used for the Ru atom and the 6-31G** basis set[22] was used for all other atoms. Geometry optimizations in the ground state (S0) and lowest-lying triplet state (T0) were performed in the gas phase and the nature of all stationary points was confirmed by normal mode analysis. The conductor-like polarizable continuum model method (CPCM)[23] with water as solvent was used to calculate the electronic structure and the excited states in solution. Fifty singlet excited states and the corresponding oscillator strengths were determined with a Time-Dependent Density Functional Theory (TD-DFT)[24] calculation. Eight triplet excited states were calculated by TD-DFT using the lowest-lying triplet state geometry. The electronic distribution and the localization of the singlet and triplet excited states were visualized using the electron density difference maps (EDDMs).[25] GaussSum1.05[26] was used for EDDMs calculations and for the electronic spectrum simulation. A full summary of the computational results is reported in the Supporting Information.

DNA Binding Kinetics. Reaction mixtures of DNA and complexes $[(\eta^6\text{-}p\text{-cym})Ru(bpm)(Py)]^{2+}$ (**1**),

[(η^6-*p*-cym)Ru(bpm)(4,4'-bpy)]$^{2+}$ (**4**) and [(η^6-*p*-cym)Ru(phen)(Py)]$^{2+}$ (**10**) were prepared in three ways: (A) in the dark (henceforth referred to as 'non-irradiated'), (B) following the addition to DNA of previously irradiated **1**, **4** and **10** ('pre-irradiated'), or (C) by addition of **1**, **4** and **10** to DNA followed by photoirradiation of the resulting mixture ('irradiated'). The samples were photoirradiated with white light (λ_{irr} = 400−660 nm) at selected photoirradiation times. The binding kinetics experiments with CT-DNA were then performed as described. Calf thymus DNA (CT-DNA) and plasmid DNAs were incubated with **1**, **4** and **10** or platinum complexes (cisplatin, transplatin and diethylenediamine platinum) in 10 mM $NaClO_4$ (pH ≈ 6) at 310 K for 24 h. For each individual assay the values of r_b (r_b is the number of atoms of the metal bound per nucleotide residue) were determined by Flameless Atomic Absorption Spectrometry (FAAS). CT-DNA (42% G + C, mean molecular mass *ca.* 20000 kD) was prepared and characterised as described previously.[27] Plasmids, pUC19 [2686 base pairs (bp)] and pSP73KB (2455 bp) were isolated according to standard procedures.

DNA Transcription by RNA Polymerase *In Vitro*. Transcription of the (*Nde*I/*Hpa*I) restriction fragment of pSP73KB DNA with T7 RNA polymerase and electrophoretic analysis of the transcripts were performed with complexes **1**, **4** and **10** according to the protocols recommended by Promega (Promega Protocols and Applications, 43−46 (1989/90).[28] The DNA concentration used was 7.8 × 10^{-5} M (0.5 μg/20 μL) (related to the monomeric nucleotide content).

Unwinding of Negatively Supercoiled DNA. Unwinding of closed circular supercoiled pUC19 plasmid DNA was assayed by an agarose gel mobility shift assay.[29] The mean unwinding angle can be calculated from the equation $\Phi = -18\sigma/r_b(c)$, where σ is the superhelical density (representing the number of turns added or removed relative to the total number of turns in the relaxed plasmid, indicating the level of supercoiling), and $r_b(c)$ is the r_b value at which the supercoiled and nicked forms co-migrate.[30] Samples of plasmid DNA at a concentration of 1.0 × 10^{-4} M (0.5 μg/15 μL) (related to the monomeric nucleotide content) were incubated with the Ru^{II} complexes at 310 K for 24 h. The pre-irradiated forms of **1**, **4** and **10** (irradiation for 24 h) of the Ru^{II} arene pyridine complexes were used. All

samples were precipitated by ethanol and redissolved in the TAE (Tris-aceate/EDTA, pH ≈ 8.0) buffer to remove free, unbound Ru^{II} arene complexes. One aliquot of the precipitated sample was subjected to electrophoresis on 1% agarose gels running at 298 K with TAE buffer and the voltage was set at 25 V. The gels were then stained with ethidium bromide (EtBr), followed by photography with a transilluminator. Electron absorption spectrometry (EAS) and/or Flameless atomic absorption spectroscopy (FAAS) were used for the determination of r_b values.

DNA Melting Temperature. CT-DNA at the concentration of 32 μg/mL was modified by Ru^{II} arene complexes at various r_b values in 10 mM $NaClO_4$ with 1 mM Tris-HCl/0.1 mM EDTA and pH = 7.4 at 310 K for 24 h. The samples were then dialysed and the r_b was determined by EAS and FAAS. The salt concentration was then further adjusted by the addition of $NaClO_4$ to values in the range of 0.01−0.22 M. The melting curves of CT-DNA were recorded by measuring the absorbance at 260 nm. The value of the melting temperature (t_m) was determined as the temperature corresponding to a maximum on the first-derivative profile of the melting curves. The t_m values could be thus determined with an accuracy of ± 0.5 °C.

Circular Dichroism (CD). Isothermal CD spectra of CT-DNA modified by **1**, **4** and **10** at the concentration of 3.3×10^{-4} M were recorded at 298 K in 10 mM $NaClO_4$ by using a Jasco J-720 spectropolarimeter equipped with a thermoelectrically controlled cell holder. The cell pathlength was 1 cm. CD spectra were recorded in the range of 230−600 nm in 0.5 nm increments with an averaging time of 0.5 s.

Flow Linear Dichroism (LD). Flow LD spectra were collected by using a flow Couette cell in a Jasco J-720 spectropolarimeter adapted for LD measurements. The flow cell consists of a fixed outer cylinder and a rotating solid quartz inner cylinder, separated by a gap of 0.2 mm, giving a total pathlength of 1 mm. LD spectra of DNA at the concentration 3.3×10^{-4} M modified by **1**, **4** and **10** were recorded at 298 K in 10 mM $NaClO_4$.

Ethidium Bromide (EtBr) Fluorescence. Measurements were performed on a Varian Cary Eclipse

spectrofluorimeter using a 1-cm pathlength quartz cell. Fluorescence measurements of CT-DNA modified by **1**, **4** and **10** in the presence of EtBr were performed at an excitation wavelength of 546 nm, and the emitted fluorescence was analyzed at 590 nm. The fluorescence intensity was measured at 298 K in 0.4 M NaCl to avoid secondary binding of EtBr to DNA.[31] The concentrations were 0.01 mg/mL for DNA and 0.04 mg/mL for EtBr, which corresponded to the saturation of all intercalation sites for EtBr in DNA.[32]

Other Physical Methods. The FAAS measurements were carried out on a Varian AA240Z Zeeman atomic absorption spectrometer equipped with a GTA 120 graphite tube atomizer. The PAA gels were visualized by using a BAS 2500 FUJIFILM bioimaging analyzer, with the AIDA image analyzer software (Raytest, Germany).

Cancer Cell Growth Inhibition. The A2780 human ovarian cancer cell line was obtained from the ECACC (European Collection of Animal Cell Cultures, Salisbury, UK). The cells were maintained in RPMI 1640 media (supplemented with 10% fetal calf serum, 1% L-glutamine, and 1% penicillin/streptomycin). All cells were grown at 310 K in a humidified atmosphere containing 5% CO_2. After plating, human ovarian A2780 were treated with the Ru^{II} arene complexes **1**, **3**, **4**, **8**, **9**, **10**, **12**, **15** and **16** on day 3 at concentrations ranging from 0.1 to 100 μM. Solutions of the Ru^{II} complexes were made up in ambient light conditions in 0.125% DMSO to assist dissolution (0.03% final concentration of DMSO per well in the 96-well plate). Cells were exposed to the complexes for 24 h, washed, supplied with fresh medium, allowed to grow for three doubling times (72 h), and then the protein content measured (proportional to cell survival) using the sulforhodamine B (SRB) assay.[33]

Results

Synthesis and X-ray Crystal Structures. The complexes $[(\eta^6\text{-arene})Ru(N,N')(L)]^{2+}$ studied in this work are shown in Figure 1. The dicationic Ru^{II} arene complexes **1**−**16** were synthesized as PF_6 salts in good yields (>50% in almost all cases). The synthetic route involved the reaction of the corresponding

[(η^6-arene)Ru(N,N')Cl][PF_6] complex with $AgNO_3$ in a 1:1 mixture of MeOH/H_2O to afford the corresponding aqua species [(η^6-arene)Ru(N,N')(OH_2)]$^{2+}$, to which an excess of the appropriate ligand L and KPF_6 were added. All the synthesized complexes were fully characterized by spectroscopic and analytical methods.

The molecular structure of complexes **2**, **6**, **7**, **10**, and **13** were determined by single crystal X-ray diffraction. Selected bond lengths and angles are given in Table 1, the structures with numbering schemes are shown in Figure 2, and the crystallographic data are listed in Table S1. These complexes have very similar structural features between them and are found to adopt the familiar pseudo-octahedral three-legged piano stool geometry common to other Ru^{II} arene structures,[10] with the Ru atom π-bonded to the arene ligand (*p*-cym in **2**, **6**, **7**, and **10**; ind in **13**), coordinated to a pyridine nitrogen (**2**, **6**, **7**, **10**, and **13**), and to two nitrogen atoms of the chelating ligand (bpm for **2**, **6**, and **7**; phen for **10**; bpy for **13**). Details of the crystal packing, hydrogen bond and π-π stacking interactions for complexes **2**, **6**, **7**; **10** and **13** are reported in the Supporting Information, Figures S1-S6.

DFT Optimised-Geometry Structures and Molecular Orbitals of Ru^{II} Arene Complexes. Geometry optimization of complexes **1**−**6** and **8**−**16** shown in Figure 1, was performed for both the ground state (S0) and the lowest-lying triplet state (T0), employing the DFT method with the B3LYP functional. Complex **7** was not obtained in sufficient yields and therefore was not considered for further experimental or theoretical studies. Details of the computational results are summarized in the Supporting Information (Tables S2 and S3).

Ground State (S0) Geometry. All the DFT geometry-optimised Ru^{II} arene complexes have a pseudo-octahedral structure in the ground-state (S0). The overall agreement with the experimental data was satisfactory, however in few cases (particularly for complexes **2** and **6**) the functional used was found to underestimate the Ru−$N_{(L)}$ bond distances by *ca*. 0.01−0.04 Å when compared to the X-ray crystal structures. Slight variations in the calculated Ru−*p*-$cym_{(centroid)}$ distances where also found when compared to those determined by X-ray crystallography, especially for complexes **10** and **13**, where the

value predicted is *ca*. 0.04 Å larger in the first case. A good agreement between calculated and experimental Ru−$N_{(N,N')}$ bond distances was found for all complexes.

Lowest-Lying Triplet State (T0) Geometry. The lowest-lying triplet states geometries were also optimised for complexes **1**−**6** and **8**−**16**, due to the key role that this state can play in their photochemistry. It was found that all complexes have similar Ru−$N_{(L)}$ distances of 2.14±0.06 Å which resemble those observed in the ground state (S0), except for complexes **1** and **5** whose distances are slightly shorter. In contrast, complexes **10** and **12** have Ru−$N_{(Py)}$ distances considerably elongated (~2.5 Å). For complexes **1**−**6**, **8**, **9**, **13** and **16** one of the Ru−N,N' bond distances in the T0 state is considerably longer than the other, typically 2.18 and 2.40 Å whereas in the remaining complexes, it resembles more to that obtained for the ground state. In almost all cases, each of the computed Ru−$arene_{(centroid)}$ distances are longer than those calculated for the ground state (~2.06 Å); complex **4** having the largest value (*ca*. 2.26 Å). Complex **11** was found to keep nearly the same geometry as in S0.

*Orbital Analysis***.** The shape of selected frontier orbitals for the Ru^{II} arene complexes **1**–**6** and **8**–**16** in the ground state S0 (Figure S7) and lowest-lying triplet state T0 (Figure S8) in the T0 geometry were calculated and analysed.

Molecular orbitals in the ground state. Complexes **1**–**6** and **8**–**16** have HOMO orbitals that are generally localized on the Ru^{II} center and on the arene ligand. A few exceptions however are present. Complexes with extended monodentate pyridine ligands (namely **3** (4-MeOPy), **4** (4,4'-bpy), **5** (4-PhPy), and **6** (4-BzPy)) show increasing contributions from the pyridine ligand to the HOMOs. In the case of **6**, the HOMO is actually fully centered on the 4-BzPy. Similarly, complex **12** shows a HOMO that is bathophen-centered. For all complexes **1**–**6** and **8**–**16**, the LUMO orbital is centered on the N,N' chelating ligand and at least one orbital among either the LUMO+1, LUMO+2 or LUMO+3 displays σ*-antibonding character towards the Ru–L and one Ru–N,N' bond. Figure 3 shows LUMO+2 for complex **10** as an example.

Molecular orbitals in the triplet state. Complexes **1**–**3**, **8**, **9** and **10** display a lowest-SOMO (*l*-SOMO)

delocalized over the whole molecule, while the highest-SOMO (*h*-SOMO) has a prevalent Ru-arene character and resembles the σ*-antibonding orbitals of the S0 geometry. For the other derivatives, the N,N'- or L-ligand character of the SOMOs is higher.

Electronic Absorption Spectra and Singlet Excited States.

The experimental UV-vis absorption spectra with the corresponding maxima (λ, nm) and extinction coefficients (ε, M^{-1} cm^{-1}) are reported in Figure S9 and Table S4. A complete set of TD-DFT calculations was performed on complexes **1**−**6** and **8**−**16** shown in Figure 1, at the B3LYP/LanL2Dz/6-31G** level to characterise their singlet excited states and electronic properties. Data for complex **3** are shown in Figure 4.

For all complexes the absorbance tail in the 380–420 nm region is dominated by metal centered (^{1}MC) and metal-to-ligand charge transfer (^{1}MLCT) transitions. Some of these transitions are partially dissociative since they have significant contributions from the Ru−N,N' and Ru−$N_{(L)}$ σ*-antibonding orbitals. Not surprisingly, a poorer agreement between the experimental spectrum and the computed singlet transitions is observed in the case of complex **12** (TD-DFT overestimates the oscillator strengths of the transitions at around 370 nm). At higher energy (*ca.* 330−250 nm), almost pure ^{1}MLCT (Ru → N,N') states are found for all complexes. However, in several cases (i.e. **10**−**12**) a more pronounced interligand (^{1}IL) or ligand-centered (^{1}LC) character is also found; complex **3** displays a maximum at 384 nm with ^{1}MC/^{1}MLCT character (the latter being predominant), a ^{1}MLCT shoulder at 300 nm and an intense peak at 247 nm of mixed ^{1}MLCT/^{1}LC nature. Selected Electron Density Difference Maps (EDDMs) for complexes **1**−**6** and **8**−**16** are shown in Figure S10−S24. The orbital compositions of computed singlet transitions for all complexes is reported in the Supporting Information Table S5−S19.

Photoirradiation of Ru^{II} arene complexes with White Light or UVA Irradiation. The behavior under white light irradiation in aqueous solution of complexes **1**−**6**, **8**−**10**, and **12**−**16** was explored. Due

to its instability in aqueous solution, photoirradiation of complex **11** was performed in an acetone solution.

In the dark, aqueous solutions of all the complexes were remarkably stable over a large range of pH* values (pH* = 2–12) and no hydrolysis reaction was observed at ambient temperature over a period of *ca*. 2 months. As shown by UV-vis data, when aqueous solutions of **1**−**6**, **8**−**10**, and **12**−**16** are photoirradiated with white light (λ_{irr} = 400−660 nm) the electronic absorption bands shift and change in intensity, the largest changes being observed around the 200−300 nm region, Figure S25. The presence of an isosbestic point at *ca*. 310 nm indicates the formation of a single photoproduct in all cases. The pH* values of the solutions were determined at the beginning and at the end of each photoirradiation experiment. In most cases a slight decrease in the values was registered, from an average of ~7.14 at the starting point down to ~6.52 at the final stage. ^{1}H NMR spectra recorded at different stages of photolysis with white light or UVA irradiation confirm that all the complexes selectively released their pyridine or pyridine-derivative ligand (L) with the subsequent *in situ* formation of the corresponding aqua adduct as the only metal-containing photoproduct. A similar behavior was previously reported by us for complex **1**.[13] Both UV-vis and ^{1}H NMR spectra for complex **10** are shown in Figure 5 as a generic example for white light irradiation; for the remaining derivatives the observed changes were identical. Assignment of ^{1}H NMR resonances was achieved using standard 2D techniques. The mass-to-charge ratios and isotopic models obtained from HR-MS spectra are consistent with the formation of the aqua complexes as the corresponding photoproducts, Table S20.

Selected Ru^{II} arene complexes (**1**, **8**−**10**, and **13**−**16**) were also photoirradiated by UVA (λ_{irr} = 320−400 nm) at 310 K and followed by UV-vis and ^{1}H NMR spectroscopy. Their UV-vis spectra are shown in Figure S26. Similar spectral changes as those produced with white light irradiation are observed, but half the time was needed. Additionally, a larger extent of photo-conversion of all the selected complexes to their corresponding aqua adducts was also achieved. Table S21 lists the

percentage of adducts detected by ^{1}H NMR after *ca*. 4−6 h of continuous UVA irradiation at 310 K for complexes **1**, **8**−**10**, and **13**−**16**. HR-MS spectra are consistent with the formation of the corresponding aqua complexes as the photoproducts, independently of the wavelength employed, Table S20.

In general, a dependence of the photoirradiation extent on the nature of the ligands around the metal centre was observed. Figures S27-S31 show and Table S22-S26 lists the percentage of species detected by ^{1}H NMR after *ca*. 10−12 h of continuous white light irradiation (λ_{irr} = 400−660 nm) at 310 K for complexes (A) **1**−**6**, (B) for complexes **8**−**9**, (C) for complexes **10**−**12**, (D) for complex **13**, (E) and for complexes **14**−**16**; complex **1** is included for comparison. Within the first group (A), complex [(η^6-*p*-cym)Ru(bpm)(4,4'-biPy)]$^{2+}$ (**4**) photoconverts at the slowest rate and to the lesser extent. Complexes **1** and **3** where L = Py and 4-MeOPy, respectively, were found to convert to a higher extent. When L is 3-AcPy (**14**), NA (**15**) or 3-AcOPy (**16**), the amount of aqua adduct generated is larger after a shorter irradiation time when compared to complex **1** (group B). Within group (C), complex **11** appeared to be unstable in aqueous media and thus was irradiated in acetone. It can be seen that after 628 and 610 min of irradiation, 75% and 60% of complexes **10** and **12**, respectively are still present intact in solution. In group D, for complexes **8** and **9** 100% photo-coversion to the aqua adduct was achieved after 305 and 425 min, respectively, but for complex **13** only 28% of photo-conversion was achieved after 643 min.

Triplet Excited States. Due to the relevance of triplet states in the photophysics and photochemistry of transition metal complexes, triplet excited states were calculated by DFT and TD-DFT. Analysis of the T0 geometry (obtained by unrestricted DFT) of complexes **1**−**6**, **8**−**10**, **12**, **13**, and **16** (shown in Figure 1) reveals that they have a distorted geometry, highlighting both an elongated Ru−N,N'$_{(bpm)}$ bond with respect to the ground state, which is typically *ca*. 0.3 Å longer, as well as an elongated Ru−N$_{(L)}$ bond in the case of complexes **2**, **3**, **5**, and **6**. The observed increase in the Ru−N distances can be ascribed to the population of σ*-antibonding *h*-SOMO that involves only one bound-N within bpm, hence dissociation

of the chelating ligand is prevented by the strong coordination of the other pyrazine ring of the ligand. In the case of complexes **1**, **4**, and **14**−**15**, no Ru−$N_{(L)}$ bond elongation is observed. Spin density surfaces (Figure S32) show that the nature of the T0 for complexes **1**−**6**, **8**−**10**, **12**, **13**, and **16** is ^{3}MC. In the case of complex **11** the lowest-lying triplet is phendio-based, while for **14** and **15** is L-centered (3-AcPy and NA, respectively).

The ^{3}MC nature of the lowest-lying triplet state for complexes **1**−**6**, **8**−**10**, **12**, **13**, and **16** was confirmed by the TD-DFT calculations on triplet transitions. ^{3}MC states and distorted triplet geometries are usually found to be in favor of non-emissive deactivation pathways and photochemical activity.[34] TD-DFT highlights that the three lowest triplet states have all ^{3}MC character, but none of them as significant contribution from σ*-antibonding orbitals. Dissociative ^{3}MC states have higher energy (Tables S27-S41 and Figures S33-S47), consistently with an inefficient photochemical conversion.

In the case of **11**, no distortions are observed when comparing ground state and triplet excited state geometries. The TD-DFT calculations show that there is a greater ^{3}MLCT character, with no significant involvement of the σ*-antibonding orbitals and the ^{3}MC states. According to TD-DFT calculations, the lowest-lying triplet state for complex **14** is ^{3}MC and has a marked dissociative nature towards the Ru−$N_{(L)}$ bond (contribution from LUMO+1 and LUMO+3), while for **15** is nicotamide (NA)-centered.

Photocontrolled Nucleobase Binding. Following our previous studies[13] and in order to investigate the ability of the [(η^6-arene)Ru(N,N')(L)][PF_6]$_2$ complexes to bind to DNA bases, an irradiation experiment with white light (λ_{irr} = 400−660 nm) at 310 K in the presence of 9-ethylguanine (9-EtG) and 9-ethyladenine (9-EtA) was performed for complexes **1**−**6**, **8**−**10**, and **12**−**16**. As shown in Figure 6 (selected example for [(η^6-*p*-cym)Ru(bpm)(4-MePy)]$^{2+}$, complex **2**), irradiation of the complexes at 310 K in D_2O in the presence of 1 mol equiv of 9-EtG resulted in the initial formation of the corresponding aqua adduct [(η^6-arene)Ru(N,N')(OH_2)]$^{2+}$ followed by coordination of the nucleobase to the Ru centre to form [(η^6-arene)Ru(N,N')(9-EtG-*N*7)]$^{2+}$. The binding to 9-EtG is not reversible upon the termination

of irradiation. Figure S48 shows the 2D ^{1}H-^{1}H NOESY spectrum which was used to assign the proton resonances and confirm the structure of [(η^6-*p*-cym)Ru(bpm)(9-EtG-*N*7)]$^{2+}$ (**15-EtG**).[13] An NOE cross-peak between H(8) of 9-EtG and the 2,2'-CH of bpm was observed, suggesting coordination of 9-EtG through *N7* as previously noted.[35] For the rest of the Ru^{II} arene complexes a similar behavior was observed when the irradiation was carried out in the presence of 9-EtG. The mass-to-charge ratios and isotopic models obtained from HR-MS spectra are consistent with the formation of the corresponding guanine adducts, Table S42. A similar irradiation experiment in the presence of 9-EtA resulted in no 9-EtA binding to the Ru centre for any of the complexes.

Photocontrolled CT-DNA Interactions in Cell-Free Media. In order to explore the possibility and nature of the interactions with DNA, the complexes [(η^6-*p*-cym)Ru(bpm)(Py)]$^{2+}$ (**1**), [(η^6-*p*-cym)Ru(bpm)(4,4'-bpy)]$^{2+}$ (**4**) and [(η^6-*p*-cym)Ru(phen)(Py)]$^{2+}$ (**10**) were selected for further studies.

DNA Binding Kinetics. The binding kinetics experiments with CT-DNA were performed as described in the experimental section. The results, summarized in Table S43, indicate that the non-irradiated forms of **1**, **4**, and **10** are not bound to DNA significantly in 10 mM $NaClO_4$ (less than 5% for **1** and **10** and *ca*. 20% of **4** after 48 h). Pre-irradiated and irradiated forms of complexes **1**, **4**, and **10** reacted with DNA to a similar extent *ca*. 40%, 54%, and 56%, respectively after 24 h. It can be seen that pre-irradiated Ru^{II} arene complexes bind faster but to the same extent as the irradiated DNA mixtures, Figure S49.

DNA Transcription by RNA Polymerase *in Vitro*. The autoradiogram of the inhibition of RNA synthesis by T7 RNA polymerase on pSP73KB DNA containing adducts of the Ru^{II} arene complexes or cisplatin is shown in Figure 7 (top). The bands corresponding to the transcription of DNA modified by the non-irradiated forms of complexes **1**, **4**, and **10** are rather faint in intensity, except for complex [(η^6-*p*-cym)Ru(bpm)(4,4'-bpy)][PF_6]$_2$ (**4**), which was found to bind to DNA without irradiation (*ca*. 20%). The pre-irradiated and irradiated forms of **1**, **4**, and **10** yielded fragments of newly synthesized RNA of

defined sizes. The major stop sites produced occurred at similar positions in the gel and were exclusively at guanine residues (Figure 7, bottom) and are identical for the three Ru^{II} arene complexes. The total intensity of the bands on the autoradiogram corresponding to transcripts of single-ruthenated DNA fragments (modified to the same level, same r_b value) differed. The intensities of those corresponding to the transcription of DNA modified by the pre-irradiated forms of complexes **1**, **4** and **10** are slightly stronger than those corresponding to the irradiated forms.

Unwinding of Supercoiled pUC19 Plasmid DNA. The native agarose gel resulting from DNA modified by the Ru^{II} arene complexes **1**, **4**, and **10** in their pre-irradiated and the corresponding irradiated forms are shown in Figure 8 (top and bottom, respectively). The DNA unwinding angle produced by the adducts formed by pre-irradiated and irradiated forms of the Ru^{II} arene complexes **1** and **4**, and **10** was determined to be 6.6±1.7°, 5.2±2.2°, and 6.1±2.2°, respectively. The comigration point of the modified supercoiled and nicked DNA (r_b(c) value) was reached at r_b = 0.16, 0.19 and 0.17 for complexes **1**, **4**, and **10** respectively, Table S44. From the autoradiogram it can also be noticed that an increasing amount of nicked (OC) form occurred during photoirradiation of the Ru^{II} arene complexes in the presence of DNA (irradiated form), r_b(c) for **1** and **10** is not changed whereas DNA is significantly more nicked with increasing ruthenation in the case of **4**.

DNA Melting Temperature. The observed trend for the three complexes **1**, **4** and **10** is a constant oscillation of the t_m values, Table S45. The t_m changes are relatively small and a slight stabilization effect is observed at low ionic strengths. At the highest ionic strength, a tendency for a slight destabilization was observed.

Circular Dichroism (CD). CD spectra of DNA modified by complexes **1**, **4** and **10** (at 298 K in 10 mM $NaClO_4$) were also recorded at r_b values in the range of 0.010−0.125. As can be seen from Figure 9, the conservative CD spectrum transforms at wavelengths below 300 nm upon interaction of the three complexes with CT-DNA. There is an increase for complexes **1** and **4** and a decrease for complex **10** in the intensity of the positive band around 280 nm. The signature of complex **4** coordinated to CT-DNA is

a positive ICD centered at around 400 nm. The signature of complexes **1** and **10** bound to CT-DNA includes no such ICD. The changes in CD spectra of CT-DNA modified by Ru^{II} arene complexes **1** and **10** (at different r_b values) were monitored at 246 and 278 nm; the changes exerted by complex **4** were also monitored at 400 nm, Figure S50.

Flow Linear Dichroism (LD). Binding of all three Ru^{II} arene complexes to CT-DNA was also monitored by linear dichroism spectroscopy, Figure 10. The magnitudes of the LD signals at 258 nm decrease as a function of r_b for the irradiated forms of Ru^{II} arene complexes **1**, **4** and **10**. The changes in the LD spectrum of CT-DNA modified by complexes **1**, **4**, and **10** (at different r_b values) were monitored at 258.5 nm, Figure S51. The largest changes are induced by complex **4.** Complexes **1** and **10** behave similarly and within the same range.

Ethidium Bromide (EtBr) Fluorescence. The ability of complexes to displace the DNA intercalator EtBr from CT-DNA, was probed by monitoring the relative fluorescence of the EtBr-DNA adduct after treating the DNA with varying concentrations of the Ru^{II} arene complexes **1**, **4** and **10** in their irradiated forms. Figure 11 shows a plot of relative fluorescence *versus* r_b for the three Ru^{II} arene complexes along with cisplatin, transplatin and monofunctional chlorodiethylenetriamineplatinum(II) chloride. All three adducts of the Ru^{II} arene complexes decreased the EtBr fluorescence.

Cancer Cell Growth Inhibition (IC_{50} Values). The IC_{50} values with no irradiation provided for the Ru^{II} arene complexes (**1**−**6** and **8**−**16**) against the A2780 human ovarian cancer cell line are given in Table 2. In general, the complexes were moderately active and their potencies vary in several orders of magnitude. The most potent complex $[(\eta^6\text{-p-cym})Ru(bathophen)(Py)][PF_6]_2$ (**12**) had an IC_{50} value of 7.4 μM, comparable to that of cisplatin (2.2 μM) under the same conditions. As a general trend, the most active complexes contain *p*-cym as the arene and bpm as the N,N' chelating ligand. A change in the arene and chelating ligand to ind or hmb and phen in complexes **8**, **9** and **10**, respectively was found to decrease the activity. Within the cytotoxic series of compounds, complexes that displayed activity have either Py or 3-(substituted)Py as the L group, the Py-bearing complexes being the most active.

Discussion

X-ray Crystal Structures. The X-ray crystal structures of **2**, **6**, **7**, **10** and **13** are the first reported examples of half-sandwich complexes of the form $[(\eta^6\text{-arene})Ru(N,N')(L)]^{2+}$ where L is 4-MePy (**2**), 4-BzPy (**6**), trz (**7**), or Py (**10**, **13**). The overall structures of the complexes do not differ greatly from each other. The corresponding bond lengths and angles are comparable to analogous Ru^{II} arene complexes containing N,N' chelated ligands.[21] Neither the nature of the corresponding N,N'-chelating ligand nor the N-σ-donor, have an influence on the corresponding Ru^{II}–$arene_{(centroid)}$ distances (~ 1.70 Å). Interestingly, for all the complexes, one of the Ru–N,N' bonds is always longer than the other. A close inspection of the $Ru–N_L$ bond lengths for complexes **2** and **6** reveals no significant difference between them. A larger distortion from planarity on the bpm ligand is found for **2** compared to **6** (7.09°, and 6.80°, respectively). The nature of the arene does not influence significantly the $Ru–N,N'_{(bpm)}$ bond lengths.

Photochemistry. The photochemistry in aqueous solution at 310 K of the Ru^{II} arene complexes **1**−**6**, **8**−**10**, and **12**−**16** was investigated under white light (λ_{irr} = 400−660 nm) or UVA (λ_{irr} = 320−400 nm) irradiation using both experimental (UV-vis and ^{1}H NMR spectroscopies) as well as theoretical methods (DFT and TD-DFT calculations). The experimental results showed that this family of Ru^{II} arene complexes can selectively and exclusively dissociate the monodentate ligand (L) when excited with white light or UVA irradiation while the corresponding bound arenes and chelating ligands remain intact. It was observed that with the use of UVA irradiation, the formation of the corresponding aqua adduct can be achieved in a shorter period of time and the process is much more efficient than when white light is employed. This evidence is in good agreement with the more intense absorption bands in the UV-region of the absorption spectrum displayed by all the Ru^{II} arene complexes studied. The presence of isosbestic points in their UV-vis absorption spectra and resonances corresponding to Ru-OH_2 adduct and free L in the ^{1}HNMR spectra are consistent with the formation of a single photo-

product in all cases. It is clear that since the Ru−OH_2 species does not form in the dark, the photoactivation of the complexes allows strict control over Ru−$N_{(L)}$ bond hydrolysis reaction. Their remarkable behavior contrasts to that observed for the complexes of the form $[(\eta^6\text{-arene})Ru(L)_3]^{2+}$ where arene = benzene, toluene, or isopropyltoluene; and L = NH_3 or H_2O, for which white light irradiation in aqueous solution leads in each case to substitution of the arene as the only observable photoreaction (to produce $[Ru(OH_2)_3L_3]^{2+}$ and the corresponding free arene).[36]

As shown by the TD-DFT calculations, the selective photochemical dissociation of the L ligand is consistent with the presence of σ*-antibonding orbitals (typically the LUMO+3) which participate in several singlet and triplet transitions. On the basis of the DFT results, as well as photochemistry rates, triplet states are believed to play a key role in the ligand photodissociation mechanism of these Ru^{II} arene complexes. In fact, despite the presence of some dissociative singlet excited states, the slow formation of the Ru−OH_2 species (more than 10 h of photoirradiation with white light in some cases) confirms this hypothesis. As in the case of other Ru^{II} (poly)pyridyl complexes, a distorted lowest-lying triplet geometry[37,38] and accessible dissociative triplet excited states yield free ligand molecules and a Ru^{II} (poly)pyridyl residue, generally an aqua or solvento complex.

From the computational point of view, it is believed that all the Ru^{II} pyridine complexes studied in this work follow a relatively similar photoinduced ligand dissociation mechanism. It is likely that this dissociation occurs from a series of ^{3}MC triplet states with dissociative character and higher energy than the lowest-lying triplet excited state (which conversely has not dissociative nature). The nature of these low-lying triplet states is also consistent with the absence of fluorescence of the complexes in solution. There is evidence that competitive radiationless decay processes are much faster than these potential photochemical processes for some d^6 metal complexes.[39] After intersystem crossing promoted by the strong spin-orbital coupling, both ^{3}MC non-dissociative and dissociative triplet states can be populated. The non-dissociative ^{3}MC states are responsible for the return of the excited molecules to the ground state, while the dissociative ^{3}MCs cause the selective dissociation of the L ligand.

An attempt to understand the relationship between the photoactivity and structure of the Ru^{II} arene pyridine and pyridine-derivative complexes was also made on the basis of the experimental data. The experimental observations can be summarized as follows,

(a) Change of the basic Py ring for a 4-substituted Py ring. More electron-donating substituents on the Py ring in the *para*-position moderately increase the extent of the photo-induced hydrolysis, whereas no effect on the rate is observed.

(b) Change of the basic Py ring for a 3-substituted Py ring. Both the extent and the rate of photo-induced hydrolysis decrease on changing the *meta*-substituent on the Py ring following the order ketone > amide ≈ ester.

(c) Change of the arene. More electron-donating substituents on the arene ring increase both the extent and the rate of photo-induced hydrolysis.

(d) Change of the N,N'-chelating ligand. The more aromatic character, the lesser the extent of photo-induced hydrolysis. However, no effect on the rate is observed.

This might be an indication that the corresponding rates and extents of the photolysis reactions could also be related to the formation of the more thermodynamically favored aqua adducts. Such a hypothesis is further supported by the experimental observations showing that the photoactivatable Ru^{II} arene complexes **8** and **9**, displayed the best rates and extent of the photo-induced hydrolysis (i.e. they generate ~100% of their corresponding aqua adduct in the less time of photoirradiation, either with white light or UVA irradiation). Also the chlorido derivatives of complexes **8** and **9** hydrolyse faster and to a larger extent when dissolved in aqueous media when compared to other-arene-bearing complexes. [40] The presence of a better electron-donating arene (such as hmb in **8** or ind in **9**) stabilizes the aqua derivatives to a greater extent than those of the other complexes.

Photocontrolled DNA Interactions in Cell-Free Media. Three complexes were selected for further studies with CT-DNA in cell free media: **1**, **4** and **10** (Figure 1). As shown in the Results section (*vide supra*), upon photoactivation the three complexes undergo a clean and selective photorelease of the

pyridine (**1**, **10**) or the pyridine-derivative ligand 4,4'-biPy (**4**) to form a monofunctional reactive aqua species $[(\eta^6\text{-}p\text{-cym})Ru(N,N')(OH_2)]^{2+}$. Although the mechanism of photoactivation of these three Ru–L complexes is very similar, their effects on DNA differ from each other (both with and without photoirradiation), particularly in the case of complex **4**, suggesting that the nature of the pyridine-derivative ligand (both when bound and when photoreleased from the metal centre) as well as the N,N' chelating ligand play a key role on the mode of interaction of these complexes. Incorporating an extended pyridine such as 4,4'-bpy (as in complex **4**) provides a low *ca*. 20% of interaction of Ru^{II} compound with DNA after 48 h in the dark (non-irradiated form), presumably of intercalative nature (see EtBr fluorescence). In comparison, less than 5% of interaction with DNA was determined for **1** and **10** after 48 h and in the non-irradiated forms. Upon photoirradiation, all the aqua adducts were found to bind to DNA at varying rates. The pre-irradiated forms of Ru complexes bind faster but to the same extent as the irradiated forms. The relatively long photoirradiation times needed to start generating the corresponding aqua adducts limits the initial binding of the Ru^{II} complexes to DNA, and in the cases of complexes **1** and **4** as soon as the full photoconversion is achieved, the overall extent does not vary significantly. The rate of binding to DNA, however, is slower than that determined for the anticancer drug cisplatin ($t_{1/2}$ *ca*. 2 h under similar conditions),[41] for which DNA binding is thought to be responsible for its cytotoxic properties. In contrast, another Ru^{II} analogue $[(\eta^6\text{-bip})Ru(en)Cl]^+$, which has also been shown to be cytotoxic to cancer cells,[9] reacts much more rapidly with DNA under similar conditions ($t_{1/2}$ *ca*. 10 min). The relatively small extent of binding of the non-irradiated forms of the Ru complexes along with the slower kinetics of binding to DNA upon photoirradiation is an advantageous characteristic that may allow more drug to reach its target *in vivo* without being deactivated by reacting with other biological molecules.

The results of the transcription mapping experiments suggest that complexes **1**, **4** and **10** bind to DNA upon photoirradiation, thus inhibiting RNA synthesis. For the pre-irradiated and irradiated forms of complexes **1**, **4**, and **10** the stopsites were only guanine residues. This phenomenon occurs in a similar

fashion and with similar stopsites to those of cisplatin and to those of the Ru^{II} complex [(η^6-bip)Ru(en)Cl]$^+$, highlighting its good agreement with the photocontrolled nucleobase binding studies which show that these complexes bind significantly to 9-EtG but do not bind to 9-EtA. DNA binding upon irradiation of Ru^{II} complexes **1**, **4** and **10**, results in a low degree of unwinding (6–7°) which is very similar for the three complexes but smaller than that observed for the Ru^{II} complexes [(η^6-arene)Ru(en)Cl]$^+$ (in the range of 7 to 14°).[30] The unwinding angles produced by the adducts of Ru^{II} arene compounds **1**, **4** and **10** resemble more to those produced by monofunctional cisplatin adducts (6° and 13° for mono or bifunctional adducts, respectively).[42] The binding of the Ru^{II} arene compounds **1**, **4** and **10** to DNA upon photoirradiation affects to some extent its melting behavior. It is likely that some conformational distortions due to the formation of mono-adducts will destabilize the helix, as has been consistently observed in earlier studies with various other Ru^{II} and platinum compounds. The t_m changes induced by the Ru^{II} arene compounds **1**, **4** and **10** in the irradiated forms are however, small. It is possible that the fluctuations in the t_m values are a consequence of the DNA adducts being unstable at higher ionic strengths and temperatures, which in turn could be associated with a stabilizing effect arising from non-covalent interactions of the aromatic ligands with the duplex (arene or N,N' chelating). This hypothesis could be further supported by both the exhibited DNA unwinding angles (7^o is a typical unwinding angle for monofunctional binders), the quenching of EtBr fluorescence, and the overall positive charge on these Ru^{II} arene compounds. The magnitudes of the LD signals at 258 nm decrease as a function of r_b for all Ru^{II} arene complexes in the irradiated forms. These results suggest that the formation of DNA adducts might be accompanied by the appearance of conformational changes at the site of the lesion. CD spectra showed that the binding of complexes **1** and **4** to DNA (together with the concomitant release of pyridine or 4,4'-biPy upon photoirradiation) results in conformational alterations in double-helical DNA of a non-denaturational character, similar to those induced in DNA by antitumor cisplatin. In contrast, upon photoirradiation, the binding of **10** to DNA (accompanied by the photorelease of Py) results in conformational alterations in DNA of a denaturational character, similar to

those induced in DNA by clinically ineffective transplatin. The signature of complex **4** coordinated to CT-DNA is a positive ICD centred at around 400 nm. This could imply that the molecules become oriented as a consequence of their noncovalent interactions with DNA favoured most probably with the phen ligand over bpm.

Cancer Cell Growth Inhibition (IC_{50} Values). Complexes containing **2**, **5**, **6**, **13** and **14** (Figure 1) were non cytotoxic against the A2780 human ovarian cancer cell line under ambient light conditions up to the maximum concentration tested (100 μM). It has been previously observed a loss of cytotoxicity in ambient light conditions towards cancer cells for complexes of the type $[(\eta^6\text{-hmb})Ru(en)(X)]^+$ when X is replaced by Py.[11] The loss of activity in this complex is assumed to arise from its negligible aquation believed to be the first step towards anticancer activity. The discovery of complexes that do not hydrolyze over a large period of time but retain significant cytotoxicity implies a different mechanism of action for complexes **1**, **3**, **4**, **8**, **9**, **10**, **12**, **15**, and **16**. The cytotoxicity of several isomers of $[Ru(azpy)_2(bipy)]^{2+}$ incapable of hydrolysis has been reported,[43] as has the significant anticancer activity for the complex $[(\eta^6\text{-hmb})Ru(en)(SPh)]^{2+}$ which does not undergo hydrolysis.[11]

Conclusions

This work provides the first example of a family of piano-stool Ru^{II} arene complexes of the form $[(\eta^6\text{-arene})Ru(N,N')(L)]^{2+}$ (where N,N' is a chelating ligand and L is a pyridine or a pyridine-derivative) that can selectively photodissociate the monodentate ligand (L) when excited with UVA or white light. Such a unique feature allows control of the hydrolysis reaction of the complexes and, therefore, the formation of a reactive aqua species that otherwise would not form in the dark. Insights in the photophysical and photochemical behavior of this series of compounds were obtained by combining experimental and theoretical techniques. The process proved to be much more efficient when UVA-range irradiation was used and an initial structure-photoactivity relationship was established. The presence of a stronger electron-donating arene (such as hmb in **8** or ind in **9**) could help stabilizing the aqua derivatives to a

greater extent than those of the other complexes so that their generation is promoted. As demonstrated from the experiments of interactions with 9-EtG and 9-EtA, light activation can be used to phototrigger binding of these potential anticancer agents with discriminating preference towards 9-EtG. In order to investigate also the possibility of phototriggering the binding to DNA of the Ru^{II} arene pyridine or pyridine-derivative complexes, studies on CT-DNA interactions in cell-free media were carried out. The CT-DNA binding studies show that complexes **1**, **4** and **10** (Figure 1) in the pre-irradiated forms bind faster but to the same extent as the irradiated forms. The non-irradiated forms, as expected, bind negligibly. Further results on DNA interactions in cell-free media strengthen the case for combined monofunctional coordination and intercalation binding modes of complexes **1**, **4** and **10** upon photoirradiation. Under the premise that hydrolysis is known to be one mechanism which provides a pathway for cytotoxicity, we were not able to establish an obvious mechanism of action which would account for the cytotoxicity of these Ru^{II} arene pyridine or pyridine-derivative complexes in the absence of photoirradiation. Therefore, there is the possibility that the intact cations might exert a cytotoxic effect by other mechanisms which are currently being investigated. These encouraging results indicate that the photochemistry of these Ru^{II} arene complexes can be exploited to integrate them with the promising biological properties inherent in half-sandwich Ru^{II} complexes, thus increasing their potential as anticancer agents.

Acknowledgments. S.B.-L. thanks WPRS/ORSAS (UK) and CONACyT (Mexico) for funding. L.S. was supported by the Marie Curie Intra European Fellowship 220281 PHOTORUACD within the 7^{th} European Community Framework Programme and ERC BIOINCMED (grant no 247450 to PJS). We also thank ERDF and AWM for Science City funding, Dr Ivan Prokes of the University of Warwick for his help with NMR as well as Dr Lijiang Song and Mr. Philip Aston of the University of Warwick for their help MS instruments. Research of B. L., O. N. and V. B. was supported by the Czech Science

Foundation (Grant 301/09/H004) and the Academy of Sciences of the CR (Grant M200040901).

Supporting Information Available. Details of the preparation of complexes, crystallographic data (Table S1), selected calculated bond distances in the ground state (S0) and lowest-lying triple state (T0) (Tables S2 and S3), wavelength of absorption maxima (λ, nm) and extinction coefficients (ε, M^{-1} cm^{-1}) (Table S4), selected TDDFT singlet transitions for the Ru^{II} complexes (Tables S5-S19), mass-to-charge ratios obtained from HR-MS spectra for the photolysis products of Ru^{II} arene complexes (Table S20), percentage of species present after selected times of photoirradiation (Tables S21-S26), selected TDDFT triplet transitions for Ru^{II} complexes in the lowest-lying triplet-state optimized geometry (Tables S27-S41), mass-to-charge ratios obtained from HR-MS spectra for the photolysis products of Ru^{II} arene complexes in the presence of 9-EtG (Table S42), details of the cell-free media DNA interactions (Tables S43-S45). Selected views of the X-ray crystal structures of Ru^{II} arene complexes (Figures S1-S6), calculated *lowest*- and *highest*- Single Occupied Molecular Orbitals (Figures S7-S8), experimental UV-Vis spectrum of the Ru^{II} complexes (Figure S9), selected Electron Difference Density Maps (EDDMs) of singlet excited state transitions of Ru^{II} complexes (Figures S10-S24), UV-vis absorption spectra of the photolysis reaction of Ru^{II} arene complexes (Figures S25-S26), comparison chart showing the percentage of species formed after the photoirradiation of Ru^{II} arene complexes (Figures S27-S31), selected Electron Difference Density Maps (EDDMS) of triplet excited state transitions of Ru^{II} arene complexes (Figures S32-S47), ^{1}H-^{1}H NOESY NMR spectrum of [(η^6-*p*-cym)Ru(bpm)(9-EtG-*N7*)]$^{2+}$ (**15**) (Figure S48), cell-free media DNA studies (Tables S6 and S7) Figure S49-S51).

References

1. Farrer, N. J.; Salassa, L.; Sadler, P. J. *Dalton Trans.*, **2009**, 10690–10701.

2. (a) Sutin, N.; Creutz, C. *Pure. Appl. Chem.*, **1980**, *52*, 2717–2738; (b) Balzani, V.; Moggi, L.; Manfrin, M. F.; Bolletta, F.; Laurence, G. S. *Coord. Chem. Rev.*, **1975**, *15*, 321–433; (c) Hager, G. D.; Crosby, G. A. *J. Am. Chem. Soc.*, **1975**, *97*, 7031–7037.

3. (a) Fernández-Moreira, V.; Thorp-Greenwood, F.; Coogan, M. P. *Chem. Commun.*, **2010**, *46*, 186–202; (b) Puckett, C. A.; Barton, J. K. *Biochemistry*, **2008**, *47*, 11711–11716; (c) Zhang, C. X.; Lippard, S. J. *Curr. Opin. Chem. Biol.*, **2003**, *7*, 481–489.

4. Cosgrave, L.; Devocelle, M.; Forster, R. J.; Keyes, T. E. *Chem. Commun.*, **2010**, *46*, 103–105.

5. (a) Gill, T. P.; Mann, K. R. *Organometallics*, **1982**, *1*, 485−488; (b) Schrenk, J. L.; Palazzotto, M. C.; Mann, K. R. *Inorg. Chem.*, **1983**, *22*, 4047−4049; (c) McNair, A. M.; Schrenk, J. L.; Mann, K. R. *Inorg. Chem.*, **1984**, *23*, 2633−1640.

6. Weber, W.; Ford, P. C. *Inorg. Chem.*, **1986**, *25*, 1088−1092.

7. Bennett, M. A.; Smith, A. K. *J. Chem. Soc., Dalton Trans.*, **1974**, 233−241.

8. Magennis, S. W.; Habtemariam, A.; Nováková, O.; Henry, J. B.; Meier, S.; Parsons, S.; Oswald, I. D. H.; Brabec, V.; Sadler, P. J. *Inorg. Chem.*, **2007**, *46*, 5059−5068.

9. (a) Aird, R.; Cummings, J.; Ritchie, A.; Muir, M.; Morris, R.; Chen, H.; Sadler, P.; Jodrell, D. *Br. J. Cancer*, **2002**, *86*, 1652–1657; (b) Morris, R. E.; Aird, R. E.; Murdoch, P. D.; Chen, H. M.; Cummings, J.; Hughes, N. D.; Parsons, S.; Parkin, A.; Boyd, G.; Jodrell, D. I.; Sadler, P. J. *J. Med. Chem.*, **2001**, *44*, 3616–3621; (c) Nováková, O.; Kašpárková, J.; Bursova, V.; Hofr, C.; Vojtiskova, M.; Chen, H.; Sadler, P. J.; Brabec, V. *Chem. Biol.*, **2005**, *12*, 121–129.

10. Chen, H.; Parkinson, J. A.; Parsons, S.; Coxall, R. A.; Gould, R. O.; Sadler, P. J. *J. Am. Chem. Soc.*, **2002**, *124*, 3064−3082.

11. Wang, F.; Habtemariam, A.; van der Geer, E. P. L.; Fernández, R.; Melchart, M.; Deeth, R. J.; Aird, R.; Guichard, S.; Fabbiani, F. P. A.; Lozano-Casal, P.; Oswald, I. D. H.; Jodrell, D. I.; Parsons, S.; Sadler, P. J. *Proc. Natl. Acad. Sci. U.S.A.*, **2005**, 102, 18269−18274.

12. Peacock, A. F. A.; Habtemariam, A.; Moggach, S. A.; Prescimone, A.; Parsons, S.; Sadler, P. J. *Inorg. Chem.*, **2007**, *46*, 4049−4059.

13. Betanzos-Lara, S.; Salassa, L.; Habtemariam, A.; Sadler, P. J. *Chem. Commun*., **2009**, 6622–6624.

14. (a) Salassa, L.; Phillips, H. I. A.; Sadler, P. J. *Phys. Chem. Chem. Phys.*, **2009**, *11*, 10311–10316; (b) Salassa, L.; Garino, C.; Salassa, G.; Nervi, C.; Gobetto, R.; Lamberti, C.; Gianolio, D.; Bizzarri, R.; Sadler, P. J. *Inorg. Chem*., **2009**, *48*, 1469–1481; (c) Salassa, L.; Garino, C.; Salassa, G.; Gobetto, R.; Nervi, C. *J. Am. Chem. Soc*., **2008**, *130*, 9590–9597; (d) Cubo, L.; Pizarro, A. M.; Gómez Quiroga, A.; Salassa, L.; Navarro-Ranninger, C.; Sadler, P. J. *J. Inorg. Biochem*., **2010**, *104*, 909–918.

15. Govindaswamy, P.; Canivet, J.; Therrien, B.; Süss-Fink, G.; Štěpnička, P.; Ludvík, J. *J. Organomet. Chem.*, **2007**, *692*, 3664−3675.

16. Sheldrick, G. M. SHELXL97, University of Göttingen, Germany, **1997**.

17. (a) Sheldrick, G. M. *Acta Cryst.*, **1990**, *A46*, 467−473; (b) Sheldrick, G. M. *Acta Cryst.*, **2008**, *64*, 12−122.

18. Krezel, A.; Bal, W. *J. Inorg. Biochem.* **2004**, *98*, 161–166.

19. Frisch, M. J., et al. *Gaussian 03*, revision D 0.1; Gaussian Inc.: Wallingford CT, **2004**.

20. (a) Becke, A. D. *J. Chem. Phys.*, **1993**, *98*, 5648−5652; (b) Lee, C.; Yang, W.; Parr, R. G. *Phys. Rev. B*, **1988**, *37*, 785−789.

21. Hay, P. J.; Wadt, W. R. *J. Chem. Phys.*, **1985**, *82*, 270−283.

22. McLean, A. D.; Chandler, G. S. *J. Chem. Phys.*, **1980**, *72*, 5639−5648.

23. Cossi, M.; Rega, N.; Scalmani, G.; Barone, V. *J. Comput. Chem.*, **2003**, *24*, 669−681.

24. (a) Casida, M. E.; Jamorski, C.; Casida, K. C.; Salahub, D. R. *J. Chem. Phys.*, **1998**, *108*, 4439−4449; (b) Stratmann, R. E.; Scuseria, G. E.; Frisch, M. J. *J. Chem. Phys.*, **1998**, *109*, 8218−8224.

25. Browne, W. R.; O'Boyle, N. M.; McGarvey, J. J.; Vos, J. G. *Chem. Soc. Rev.*, **2005**, *34*, 641−663.

26. O'Boyle, N. M.; Vos, J. G., *GaussSum*, Dublin City University. Available at http://gausssum.sourceforge.net., **2005**.

27. (a) Brabec, V.; Palecek, E., *Biophysik*, **1970**, *6*, 290−300; (b) Brabec, V.; Palecek, E., *Biophys. Chem.*, **1976**, *4*, 79−92.

28. (a) Brabec, V.; Leng, M. *Proc. Natl. Acad. Sci. U.S.A.*, **1993**, *90*, 5345–5349; (b) Lemaire, M. A.; Schwartz, A.; Rahmouni, A. R.; Leng, M. *Proc. Natl. Acad. Sci. U.S.A.*, **1991**, *88*, 1982–1985.

29. Keck, M. V.; Lippard, S. J. *J. Am. Chem. Soc.*, **1992**, *114*, 3386–3390.

30. Keck, M. V.; Lippard, S. J. *J. Am. Chem. Soc.*, **1992**, *114*, 3386–3390.

31. (a) Butour, J. L.; Macquet, J. P. *Eur. J. Biochem.*, **1977**, *78*, 455–463; (b) Butour, J. L.; Alvinerie, P.; Souchard, J. P.; Colson, P.; Houssier, C.; Johnson, N. P. *Eur. J. Biochem.*, **1991**, *202*, 975−980.

32. Butour, J. L.; Macquet, J. P. *Eur. J. Biochem.*, **1977**, *78*, 455–463.

33. Skehan, P.; Storeng, R.; Scudiero, D.; Monks, A.; McMahon, J.; Vistica, D.; Warren, J. T.; Bokesch, H.; Kenney, S.; Boyd, M. R. *J. Nat. Cancer Inst.*, **1990**, *82*, 1107–1112.

34. (a) Mann, K. R.; Blough, A. M.; Schrenk, J. L.; Koefod, R. S.; Freedman, D. A.; Matachek, J. R., *Pure Appl. Chem.*, **1995**, *67*, 95−101; P. S. Wagenknecht, P. C. Ford, *Coord. Chem. Rev.*, **2011**, 591-616.

35. Yan, Y. K.; Melchart, M.; Habtemariam, A.; Sadler, P. J. *Chem. Commun.*, **2005**, 4764−4776.

36. Weber, W.; Ford, P. C. *Inorg. Chem.*, **1986**, *25*, 1088−1092.

37. (a) Pinnick, D. V.; Durham, B., *Inorg. Chem*. **1984**, *23*, 1440–1445; (b) Durham, B.; Wilson, S. R.; Hodgson, D. J.; Meyer, T. J. *J. Am. Chem. Soc*., **1980**, *102*, 600–607; (c) Collin, J. P.; Jouvenot D.; Koizumi, M.; Sauvage, J. P. *Inorg. Chem*., **2005**, *44*, 4693–4698.

38. Moucheron, C.; Kirsch-De Mesmaeker, A.; Kelly, J. M. *J. Photochem. Photobiol. B*, **1997**, *40*, 91–106.

39. (a) Pinnick, D. V.; Durham, B. *Inorg. Chem*., **1984**, *23*, 1440–1445; (b) Durham, B.; Wilson, S. R.; Hodgson, D. J.; Meyer, T. J. *J. Am. Chem. Soc*., **1980**, *102*, 600–607; (c) Collin, J. P.; Jouvenot D.; Koizumi, M.; Sauvage, J. P. *Inorg. Chem*., **2005**, *44*, 4693–4698; (d) Watts, R. J., *J. Chem. Educ*. **1983**, *60*, 834–842; (e) Baerends, E. J.; Rosa, A. *Coord. Chem. Rev*., **1998**, *177*, 97–125; (f) Vos, J. G.; Kelly, J. M. *Dalton Trans.*, **2006**, 4869–4883; (g) Farrer, N. J.; Salassa, L.; Sadler, P. J. *Dalton Trans.*, **2009**, 10690–10701.

40. Betanzos-Lara, S., PhD Thesis, University of Warwick, UK, **2010**.

41. Bancroft, D. P.; Lepre, C. A.; Lippard, S. J. *J. Am. Chem. Soc.*, **1990**, *112*, 6860–6871.

42. Kemp, S.; Wheate, N. J.; Wang, S.; Collins, J. G.; Ralph, S. F.; Day, A. I.; Higgins, V. J.; Aldrich-Wright, J. R. *J. Biol. Inorg. Chem.*, **2007**, *12*, 969–979.

43. Chen, H. M.; Parkinson, J. A.; Nováková, O.; Bella, J.; Wang, F. Y.; Dawson, A.; Gould, R.; Parsons, S.; Brabec, V.; Sadler, P. J. *Proc. Natl. Acad. Sci. U.S.A.*, **2003**, *100*, 14623–14628.

Table 1. Selected bond lengths (Å) and angles (°) for [(η^6-*p*-cym)Ru(bpm)(4MePy)][PF_6]$_2$ (**2**), [(η^6-*p*-cym)Ru(bpm)(4-BzPy)][PF_6]$_2$ (**6**), [(η^6-*p*-cym)Ru(bpm)(trz)][PF_6]$_2$ (**7**), [(η^6-*p*-cym)Ru(phen)(Py)][PF_6]$_2$ (**10**), and [(η^6-ind)Ru(bpy)(Py)][PF_6]$_2$ (**13**).

Bond length/Angle	**2**	**6**	**7**	**10**	**13**
Ru−arene$_{(centroid)}$	1.691	1.703	1.699	1.698	1.703
Ru(1)−N(13)	2.110(2)	2.121(2)	2.1041(19)	2.1169(14)	2.1250(14)
Ru(1)−N(1)	2.099(2)	2.090(2)	2.0866(18)	2.0853(13)	2.0877(13)
Ru(1)−N(8)	2.094(2)	2.094(2)	2.0808(18)	2.0970(14)	2.0727(13)
C(6)−C(7)	1.478(4)	1.479(3)	1.493(3)	1.421(2)	1.466(2)
N(8)−Ru(1)−N(1)	76.86(9)	76.93(8)	77.09(7)	78.07(5)	77.23(5)
N(13)−Ru(1)−N(8)	87.40(9)	87.96(8)	85.94(7)	85.36(5)	86.22(5)
N(13)−Ru(1)−N(1)	86.40(9)	87.43(8)	83.94(7)	87.03(5)	87.05(5)

Table 2. IC_{50} values for Ru^{II} arene complexes against the A2780 human ovarian cancer cell line in ambient light conditions.

	Compound	IC_{50} μM
(**1**)	$[(\eta^6\text{-}p\text{-cym})Ru(bpm)(Py)][PF_6]_2$	9.0
(**3**)	$[(\eta^6\text{-}p\text{-cym})Ru(bpm)(4\text{-MeOPy})][PF_6]_2$	70.0
(**4**)	$[(\eta^6\text{-}p\text{-cym})Ru(bpm)(4,4'\text{-bpy})][PF_6]_2$	61.1
(**8**)	$[(\eta^6\text{-hmb})Ru(bpm)(Py)][PF_6]_2$	23.2
(**9**)	$[(\eta^6\text{-ind})Ru(bpm)(Py)][PF_6]_2$	92.0
(**10**)	$[(\eta^6\text{-}p\text{-cym})Ru(phen)(Py)][PF_6]_2$	25.9
(**12**)	$[(\eta^6\text{-}p\text{-cym})Ru(bathophen)(Py)][PF_6]_2$	7.4
(**15**)	$[(\eta^6\text{-}p\text{-cym})Ru(bpm)(NA)][PF_6]_2$	19.0
(**16**)	$[(\eta^6\text{-}p\text{-cym})Ru(bpm)(3\text{-AcOPy})][PF_6]_2$	9.2
	Cisplatin	1.5

[a] Complexes **2**, **5**, **6**, **13** and **14** had IC_{50} values larger than 100 μM against the cell line tested (*vide supra*).

Figures Captions

Figure 1. Structures of the dicationic complexes studied in this work, synthesised as PF_6 salts.

Figure 2. X-ray structure of the cations in [(η^6-*p*-cym)Ru(bpm)(4-MePy)][PF_6]$_2$ (**2**), [(η^6-*p*-cym)Ru(bpm)(4-BzPy)][PF_6]$_2$ (**6**), [(η^6-*p*-cym)Ru(bpm)(trz)][PF_6]$_2$ (**7**), [(η^6-*p*-cym)Ru(phen)(Py)][PF_6]$_2$ (**10**), and [(η^6-ind)Ru(bpy)(Py)][PF_6]$_2$ (**13**). Thermal ellipsoids show 50% probability. The PF_6 anions and hydrogens have been omitted for clarity.

Figure 3. Calculated LUMO+2 orbital for complex [(η^6-*p*-cym)Ru(phen)(Py)][PF_6]$_2$ (**10**).

Figure 4. Experimental UV-Vis spectrum (black) for [(η^6-*p*-cym)Ru(bpm)(4-MeOPy)][PF_6]$_2$ (**3**) in aqueous solution at 310 K. Calculated singlet electronic transitions are shown as red vertical bars with heights equal to their oscillator strength.

Figure 5. Selected (A) Uv-vis and (B) ^{1}H NMR spectra of complex **10** during its aqueous photolysis (λ_{irr} = 400–660 nm). **Blue** = Py complex, **green** = aqua adduct; ★ = phen, ▲ = Py, ● = *p*-cym. Free Py is indicated with **orange** ▲.

Figure 6. ^{1}H NMR spectra recorded during the photolysis (λ_{irr} = 400−660 nm) of aqueous solutions of **2** in the presence of 9-EtG. **Blue** = [(η^6-*p*-cym)Ru(bpm)(4-MePy)]$^{2+}$, **green** = [(η^6-*p*-cym)Ru(bpm)(OH_2)]$^{2+}$, **magenta** = [(η^6-*p*-cym)Ru(bpm)(9-EtG-*N7*)]$^{2+}$; ■ = bpm, ▲ = 4-MePy, ● = *p*-cym. Free 4-MePy is indicated with **orange** ▲ and coordinated 9-EtG with **magenta** ♦.

Figure 7. Top: Autoradiogram of 6% polyacrylamide/8 M urea sequencing gel showing inhibition of RNA synthesis by T7 RNA polymerase on pSP73KB DNA containing adducts of Ru^{II} arene complexes or cisplatin. Lanes: chain terminated marker RNAs, cisplatin, at r_b = 0.02; A, U, G and C, the template modified by Ru^{II} arene compounds. **Bottom**: Schematic diagram showing the portion of the sequence used to monitor inhibition of RNA synthesis by Ru^{II} arene complexes. The arrows indicate the start of the T7 RNA polymerase, which used as template the upper strand of pSP73KB DNA, respectively. The numbers correspond to the nucleotide numbering in the sequence map of pSP73KB plasmid. (●) Indicates major stop sites for DNA modified by ruthenation.

Figure 8. The unwinding of supercoiled pUC19 plasmid DNA (1.0×10^{-4} M, 0.5 μg/15 μL) by complexes **1**, **4**, and **10** in their *pre-irradiated* forms **(top)** or by complexes **1**, **4**, and **11** in their *irradiated* forms **(bottom)**.Left and right lanes are controls (unmodified DNA); r_i values increase on going from left to right lanes; top bands correspond to the form of nicked plasmid (OC) and the bottom bands to the closed, negatively supercoiled plasmid (SC).

Figure 9. Circular dichroism (CD) spectra of CT-DNA (1×10^{-4} M) modified by Ru^{II} arene complexes **1**, **4** and **10** in their *irradiated* forms; the medium was 10 mM $NaClO_4$, pH = 6.

Figure 10. Linear dichroism spectra of CT-DNA modified by Ru^{II} arene complexes **1**, **4**, and **10**. LD spectra were recorded for DNA in 10 mM $NaClO_4$. The concentration of DNA was 2.3×10^{-4} M.

Figure 11. EtBr fluorescence *versus* r_b for DNA modified by cisplatin (●), dienPt (□), transPt (○), and Ru^{II} arene complexes **1** (■), complex **4** (△), and complex **10** (▲) in their *irradiated* forms in 10 mM $NaClO_4$ at 310 K (24h photoirradiation followed by 24 h incubation).

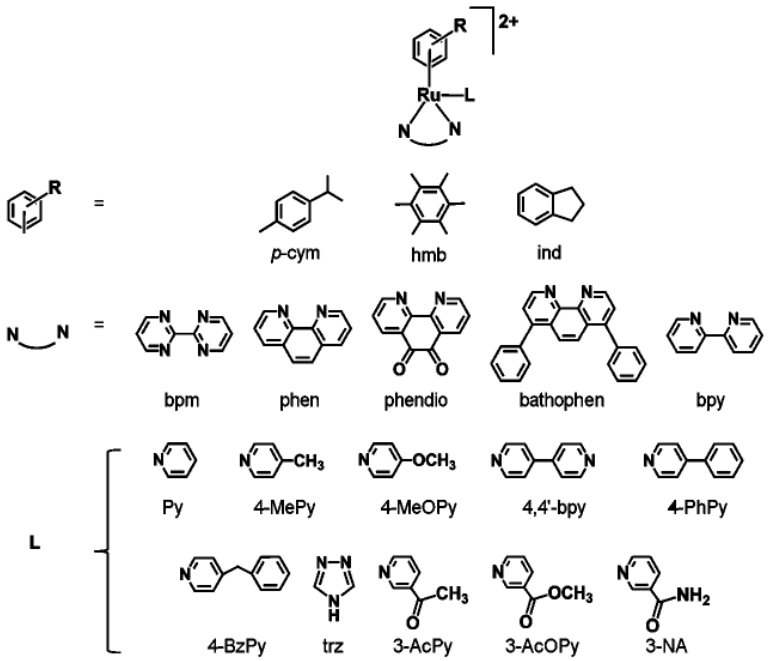

Compound	Arene	N,N'	L
(1)	*p*-cym	bpm	Py
(2)	*p*-cym	bpm	4-MePy
(3)	*p*-cym	bpm	4-MeOPy
(4)	*p*-cym	bpm	4,4'-bpy
(5)	*p*-cym	bpm	4-PhPy
(6)	*p*-cym	bpm	4-BzPy
(7)	*p*-cym	bpm	trz
(8)	hmb	bpm	Py
(9)	ind	bpm	Py
(10)	*p*-cym	phen	Py
(11)	*p*-cym	phendio	Py
(12)	*p*-cym	bathophen	Py
(13)	ind	bpy	Py
(14)	*p*-cym	bpm	3-AcPy
(15)	*p*-cym	bpm	NA
(16)	*p*-cym	bpm	3-AcOPy

Figure 1.

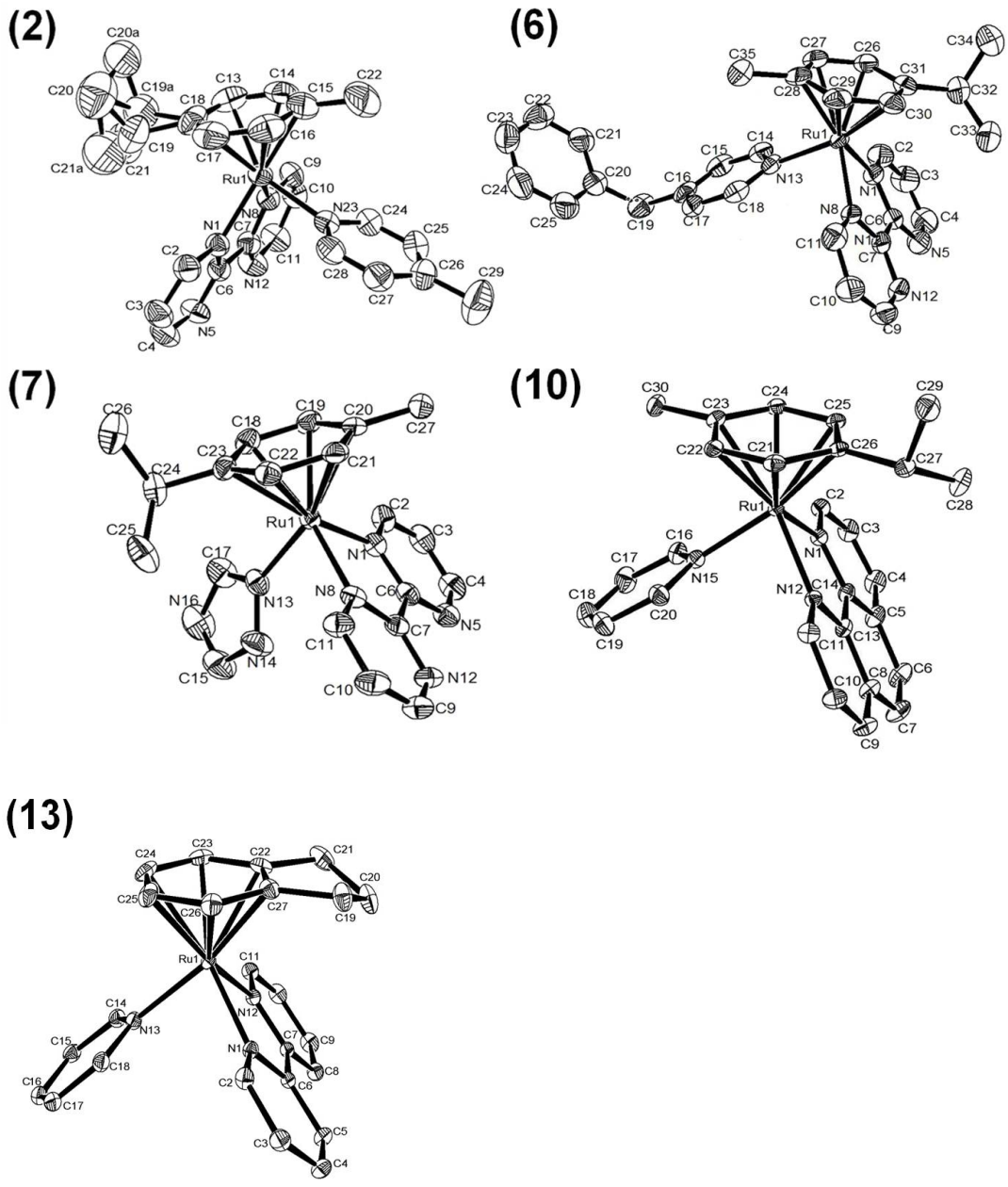

Figure 2.

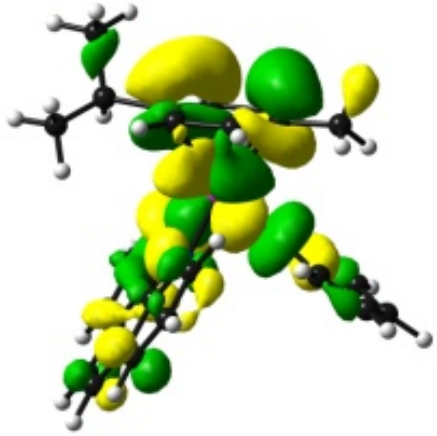

Figure 3.

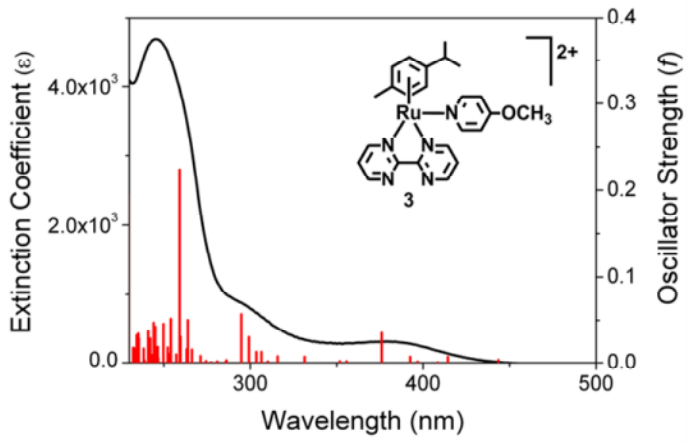
Extinction Coefficient (ε)
4.0x10^3
2.0x10^3
0.0
300
400
500
Wavelength (nm)
0.4
0.3
0.2
0.1
0.0
Oscillator Strength (f)
2+
Ru
N
OCH3
N
N
N
N
3

Figure 4.

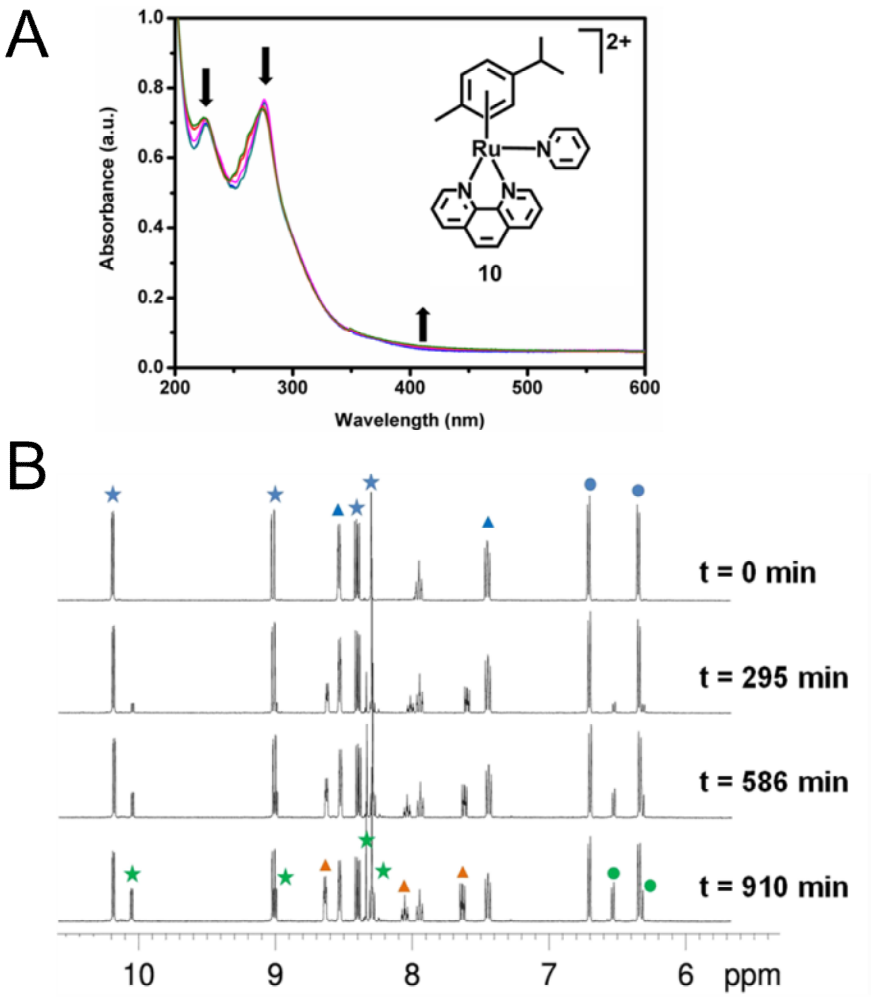
A
Absorbance (a.u.)
Wavelength (nm)
2+
Ru
N
10
B
t = 0 min
t = 295 min
t = 586 min
t = 910 min
ppm

Figure 5.

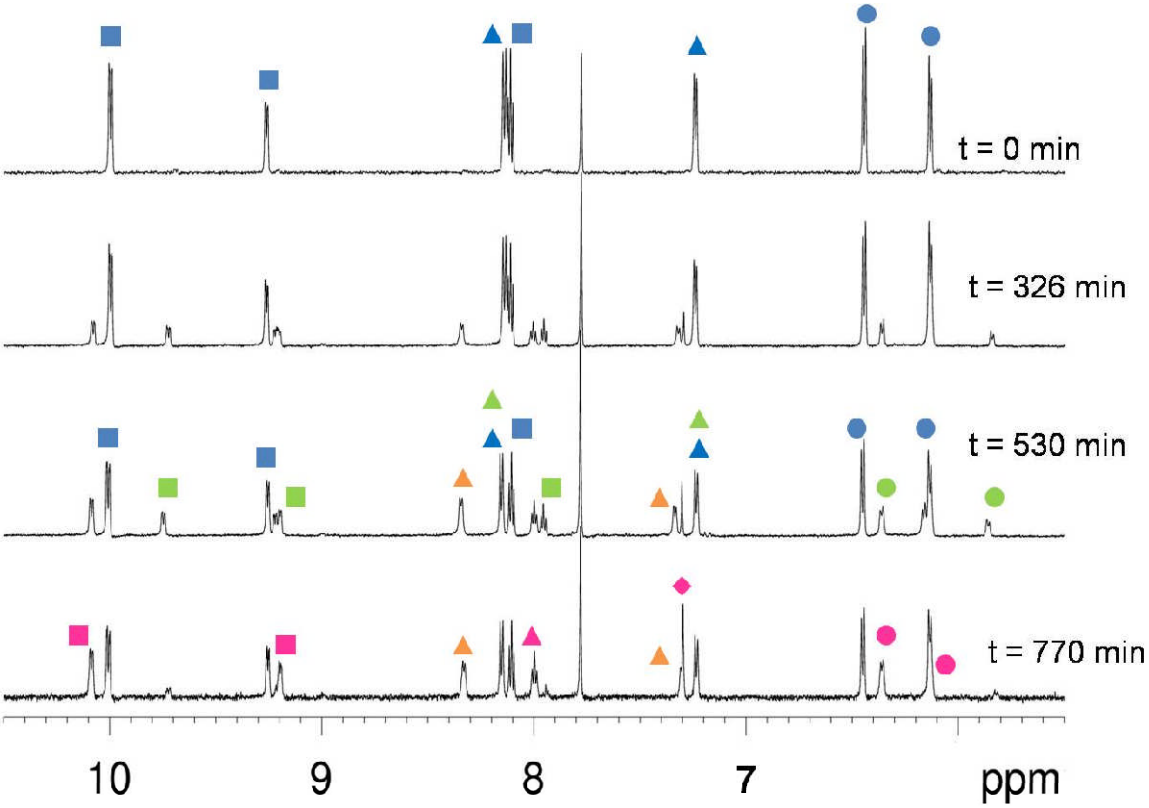

Figure 6.

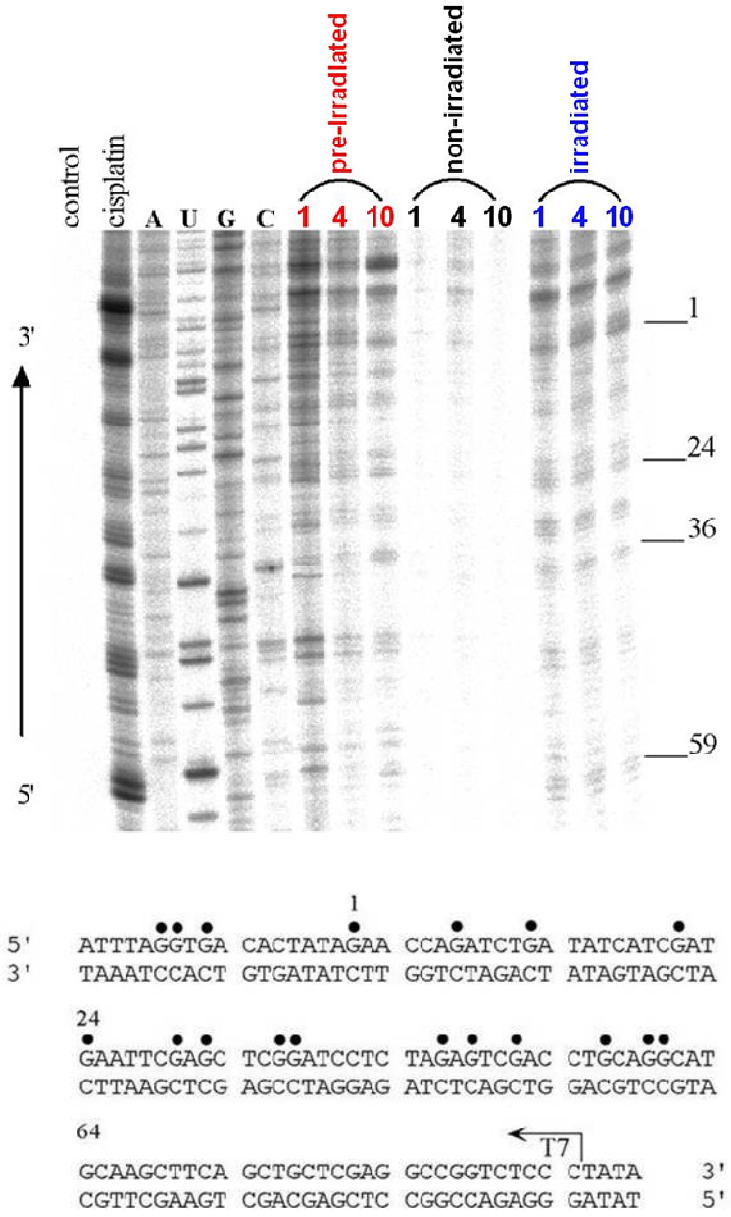
control
cisplatin
A U G C
pre-Irradiated
non-irradiated
irradiated
1 4 10 1 4 10 1 4 10
3'
5'
1
24
36
59
1
5' ATTTAGGTGA CACTATAGAA CCAGATCTGA TATCATCGAT
3' TAAATCCACT GTGATATCTT GGTCTAGACT ATAGTAGCTA
24
GAATTCGAGC TCGGATCCTC TAGAGTCGAC CTGCAGGCAT
CTTAAGCTCG AGCCTAGGAG ATCTCAGCTG GACGTCCGTA
64
T7
GCAAGCTTCA GCTGCTCGAG GCCGGTCTCC CTATA 3'
CGTTCGAAGT CGACGAGCTC CGGCCAGAGG GATAT 5'

Figure 7

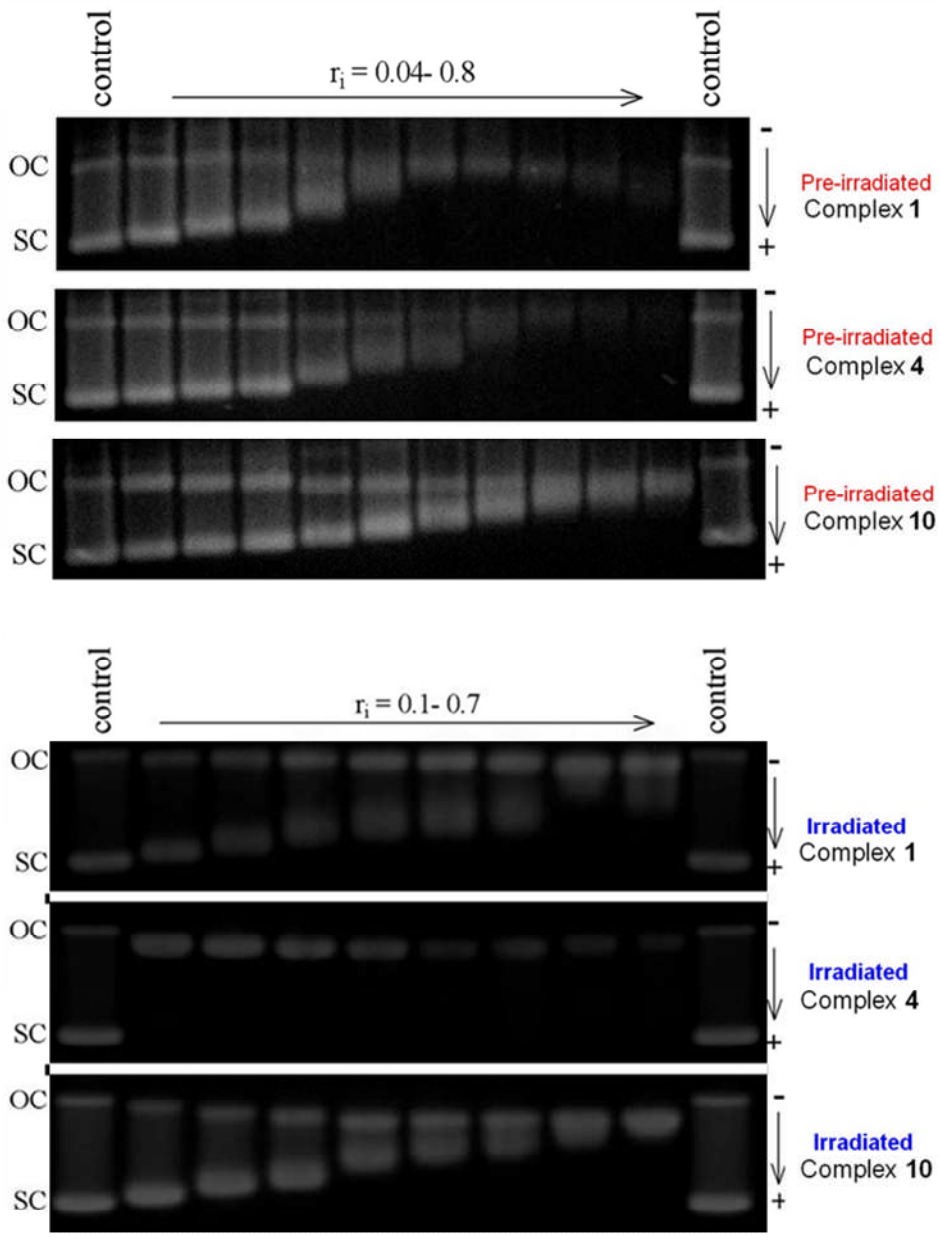
control
r_i = 0.04- 0.8
control
OC
SC
Pre-irradiated
Complex 1
Pre-irradiated
Complex 4
Pre-irradiated
Complex 10
control
r_i = 0.1- 0.7
control
Irradiated
Complex 1
Irradiated
Complex 4
Irradiated
Complex 10

Figure 8.

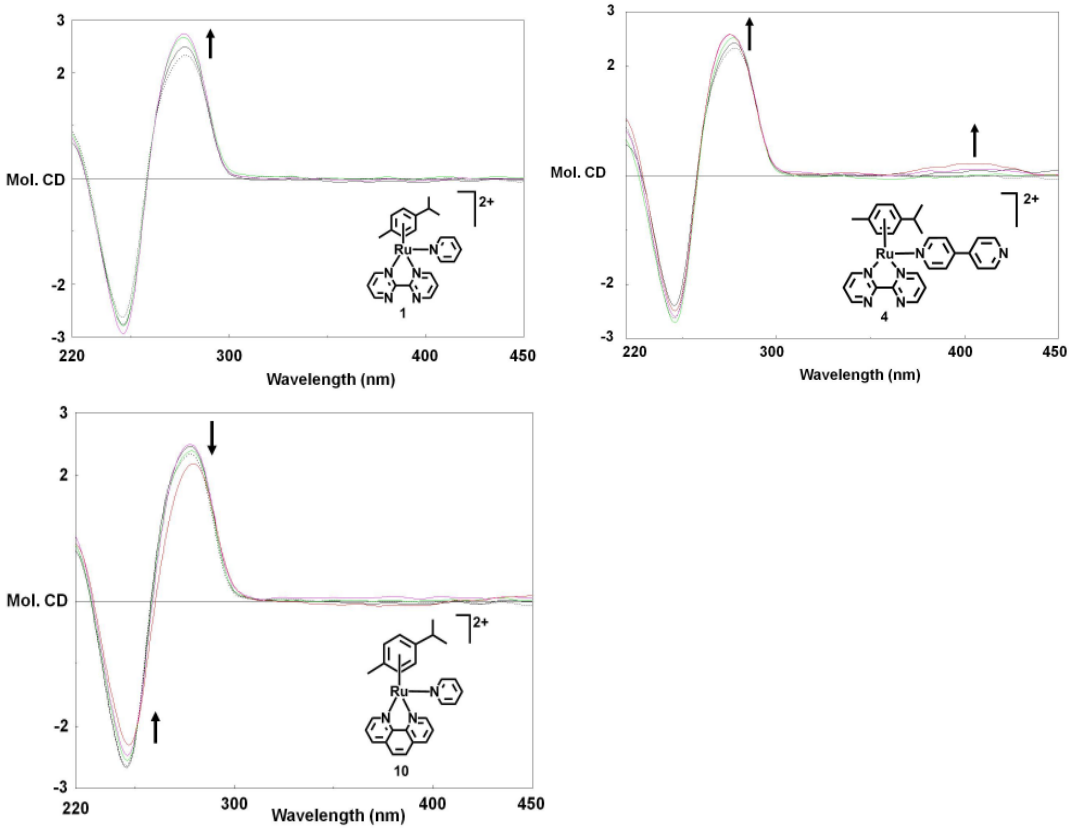

Figure 9.

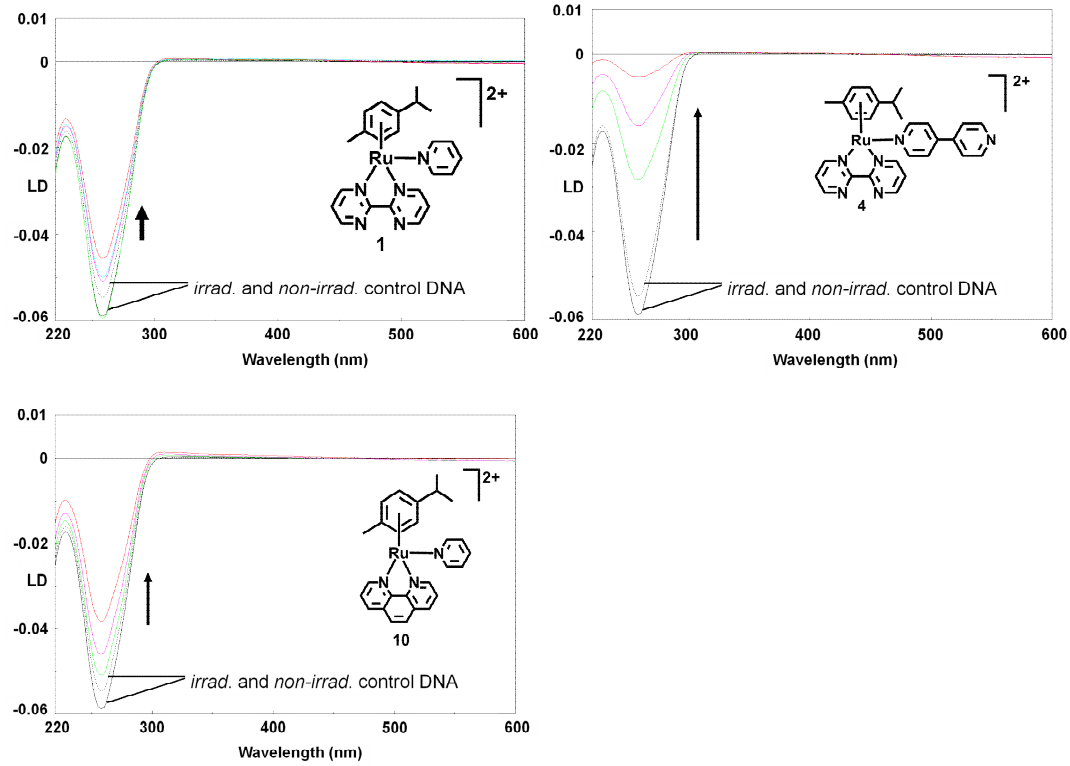
0.01
0
-0.02
LD
-0.04
-0.06
220
300
400
500
600
Wavelength (nm)
2+
Ru
N
1
irrad. and non-irrad. control DNA
4
10

Figure 10.

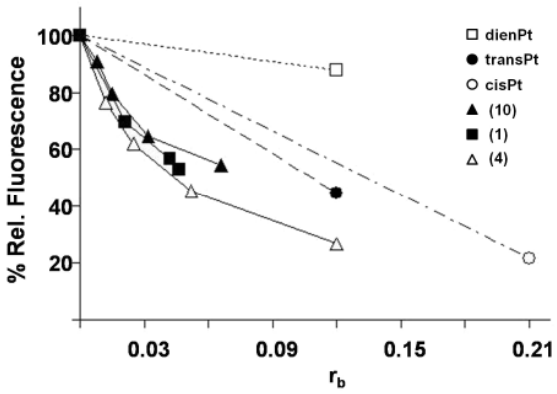
% Rel. Fluorescence
100
80
60
40
20
0.03
0.09
0.15
0.21
r_b
dienPt
transPt
cisPt
(10)
(1)
(4)

Figure 11.

TOC Graphic

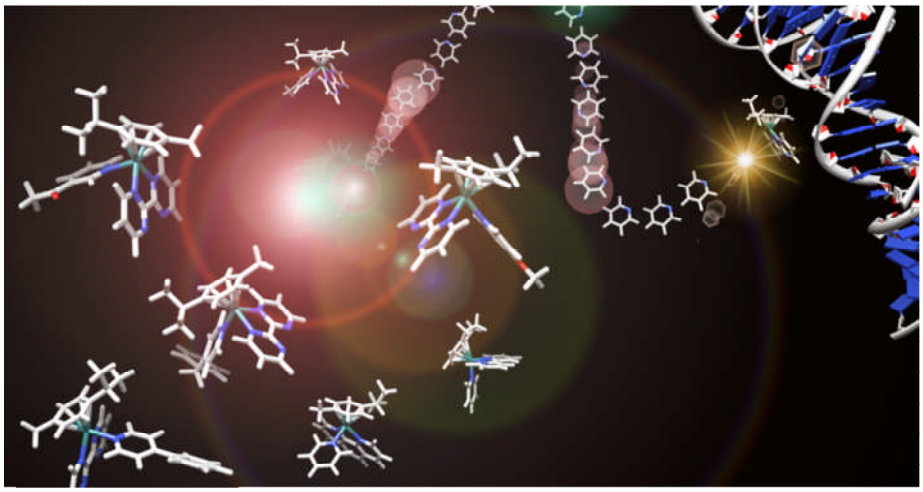

Piano-stool Ru^{II} arene complexes of the type $[(\eta^6\text{-arene})Ru(N,N')(L)][PF_6]_2$ can selectively photodissociate the monodentate ligand (L) when excited with UVA or white light allowing strict control of the formation of the reactive aqua species $[(\eta^6\text{-arene})Ru(N,N')(OH_2)]^{2+}$ that otherwise would not form in the dark. Light activation was used to photo-trigger binding of these potential anticancer agents preferentially to 9-ethylguanine (9-EtG) over 9-ethyladenine (9-EtA). Studies of reactions with calf thymus DNA in cell-free media suggest combined weak monofunctional coordinative and intercalative binding modes.